NASA TECHNICAL MEMORANDUM 109044

Fatigue Life and Crack Growth Prediction Methodology

J. C. Newman, Jr., E. P. Phillips, and R. A. Everett, Jr.

October 1993

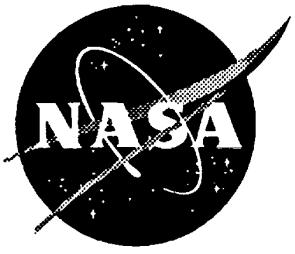

National Aeronautics and
Space Administration

LANGLEY RESEARCH CENTER
Hampton, Virginia 23681-0001

FATIGUE LIFE AND CRACK GROWTH PREDICTION METHODOLOGY

J. C. Newman, Jr.
E. P. Phillips
Mechanics of Materials Branch
NASA Langley Research Center
Hampton, Virginia 23681
USA

R. A. Everett, Jr.
Vehicle Structures Directorate
U. S. Army Research Laboratory
Hampton, Virginia 23681
USA

SUMMARY

This paper reviews the capabilities of a plasticity-induced crack-closure model and life-prediction code to predict fatigue crack growth and fatigue lives of metallic materials. Crack-tip constraint factors, to account for three-dimensional effects, were selected to correlate large-crack growth rate data as a function of the effective-stress-intensity factor range (ΔK_{eff}) under constant-amplitude loading. Some modifications to the ΔK_{eff}-rate relations were needed in the near-threshold regime to fit small-crack growth rate behavior and endurance limits. The model was then used to calculate small- and large-crack growth rates, and in some cases total fatigue lives, for several aluminum and titanium alloys under constant-amplitude, variable-amplitude, and spectrum loading. Fatigue lives were calculated using the crack-growth relations and microstructural features like those that initiated cracks. Results from the tests and analyses agreed well.

LIST OF SYMBOLS

a	Crack length in thickness (B) direction, mm
a_i	Initial defect or crack length in B-direction, mm
b	Defect or void half-height, mm
B	Specimen thickness, mm
c	Crack length in width (w) direction, mm
c_i	Initial defect or crack length in w-direction, mm
F_j	Boundary correction factor
K_{max}	Maximum stress-intensity factor, MPa$\sqrt{m}$
K_{OL}	Overload stress-intensity factor, MPa$\sqrt{m}$
K_{UL}	Underload stress-intensity factor, MPa$\sqrt{m}$
N	Number of cycles

N_f	Number of cycles to failure
R	Stress ratio (S_{min}/S_{max})
r	Notch or hole radius, mm
S	Applied stress, MPa
S'_o	Crack-opening stress, MPa
S_{max}	Maximum applied stress, MPa
S_{mf}	Mean flight stress, MPa
S_{min}	Minimum applied stress, MPa
t	Specimen thickness for through or corner crack and half-thickness for surface crack, mm
α	Constraint factor
α_g	Global constraint factor from finite-element analysis
Δc	Crack extension in c-direction, mm
ΔK	Stress-intensity factor range, MPa$\sqrt{m}$
ΔK_{eff}	Effective stress-intensity factor range, MPa$\sqrt{m}$
$(\Delta K_{eff})_{th}$	Small crack ΔK_{eff} threshold, MPa$\sqrt{m}$
ΔK_{th}	Large-crack ΔK threshold, MPa$\sqrt{m}$
ρ	Plastic-zone size, mm
σ_o	Flow stress (average of σ_{ys} and σ_u), MPa
σ_{ys}	Yield stress (0.2 percent offset), MPa
σ_u	Ultimate tensile strength, MPa
ω	Cyclic-plastic-zone size, mm

INTRODUCTION

The use of damage-tolerance and durability design concepts based on fatigue-crack growth in aircraft structures is well established (Ref 1 and 2). The safe-life approach, using standard fatigue analyses, is also used in many designs. In conventional metallic materials, crack-growth anomalies such as the small-crack effect and the various crack-tip shielding mechanisms (Ref 3 and 4) have improved our understanding of the crack-growth process but have complicated life-prediction methods. In the new metallic materials, such as the aluminum-lithium alloys, crack shielding and failure mechanisms are more complex than in conventional materials due to crack growth along tortuous crack paths (Ref 5). Over the past decade, the intense experimental studies on small or short crack growth behavior in these metallic materials have led to the realization that fatigue life of many materials is primarily "crack growth" from microstructural features,

such as inclusion particles, voids or slip-band formation. Concurrently, the improved fracture-mechanics analyses of some of the crack-tip shielding mechanisms, such as plasticity- and roughness-induced crack closure, and analyses of surface- or corner-crack configurations have led to more accurate crack growth and fatigue life prediction methods.

On the basis of linear-elastic fracture mechanics (LEFM), studies on small cracks (10 μm to 1 mm) have shown that small cracks grow much faster than would be predicted from large crack data (Ref 3 and 4). This behavior is illustrated in Figure 1, where the crack-growth rate, da/dN or dc/dN, is plotted against the linear-elastic stress-intensity factor range, ΔK. The solid (sigmoidal) curve shows typical results for large cracks in a given material and environment under constant-amplitude loading ($R = S_{min}/S_{max}$ = constant). The solid curve is usually obtained from tests with large cracks. At low growth rates, the threshold stress-intensity factor range, ΔK_{th}, is usually obtained from load-reduction (ΔK-decreasing) tests. Some typical results for small cracks in plates and at notches are shown by the dashed curves. These results show that small cracks grow at ΔK levels below the large-crack threshold and that they also can grow faster than large cracks at the same ΔK level above threshold. Small-crack effects have been shown to be more prevalent in tests which have compressive loads, such as negative stress ratios (Refs 6-8).

During the last decade, research on small- or short-crack effects has concentrated on three possible explanations for the behavior of such cracks. They are plasticity effects, metallurgical effects and crack closure (Ref 3 and 4). All of these features contribute to an inadequacy of LEFM and the use of the ΔK-concept to correlate fatigue crack growth rates.

Some of the earliest small-crack experiments were conducted at high stress levels which were expected to invalidate LEFM methods. Nonlinear or elastic-plastic fracture mechanics concepts, such as the J-integral and an empirical length parameter (Ref 9), were developed to explain the observed small-crack effects. Recent research on the use of ΔJ as a crack-driving parameter suggest that plasticity effects are small for many of the early and more recent small-crack experiments (Ref 10). But the influence of plasticity on small-crack growth and the appropriate crack-driving parameter is still being debated.

Small cracks tend to initiate in metallic materials at inclusion particles or voids, in regions of intense slip, or at weak interfaces and

grains. In these cases, metallurgical similitude (see Ref 11) breaks down for these cracks (which means that the growth rate is no longer an average taken over many grains). Thus, the local crack growth behavior is controlled by metallurgical features. If the material is markedly anisotropic (differences in modulus and yield stress in different crystallographic directions), the local grain orientation will strongly influence the rate of growth. Crack front irregularities and small particles or inclusions affect the local stresses and, therefore, the crack growth response. In the case of large cracks (which have large fronts), all of these metallurgical effects are averaged over many grains, except in very coarse-grained materials. LEFM and nonlinear fracture mechanics concepts are only beginning to explore the influence of metallurgical features on stress-intensity factors, strain-energy densities, J-integrals and other crack-driving parameters.

Very early in small-crack research, the phenomenon of fatigue-crack closure (Ref 12) was recognized as a possible explanation for rapid small-crack growth rates (see Ref 13). Fatigue crack closure is caused by residual plastic deformations left in the wake of an advancing crack. Only that portion of the load cycle for which the crack is fully open is used in computing an effective stress-intensity factor range (ΔK_{eff}) from LEFM solutions. A small crack initiating at an inclusion particle, a void or a weak grain does not have the prior plastic history to develop closure. Thus, a small crack may not be closed for as much of the loading cycle as a larger crack. If a small crack is fully open, the stress-intensity factor range is fully effective and the crack-growth rate will be greater than steady-state crack-growth rates. (A steady-state crack is one in which the residual plastic deformations and crack closure along the crack surfaces are fully developed and stabilized under steady-state loading.) Small-crack growth rates are also faster than steady-state behavior because these cracks may initiate and grow in weak microstructure. In contrast to small-crack growth behavior, the development of the large-crack threshold, as illustrated in Figure 1, has also been associated with a rise in crack-opening load as the applied load is reduced (Ref 14 and 15). Thus, the steady-state crack-growth behavior may lie between the small-crack and large-crack threshold behavior, as illustrated by the dash-dot curve.

The purpose of this paper is to review the capabilities of a plasticity-induced crack-closure model (Ref 16 and 17) to correlate and to

predict small- and large-crack growth rate behavior in several aluminum and titanium alloys under various load histories. Test results from the literature on aluminum alloys 2024-T3 (Refs 7, 18 and 19), 7075-T6 (Ref 20), LC9cs (Ref 20) and 7475-T7351 (Refs 21 and 22) and on titanium alloys Ti-6Al-4V (Ref 23 and 24), IMI-685 (Refs 23-25) and Ti-17 (Refs 23 and 24) under constant-amplitude loading were analyzed with the closure model to establish an effective stress-intensity factor range against crack growth rate relation. The effective stress-intensity factor range against crack growth rate relations were then used in the closure model to predict large-crack growth under a single spike overload, an overload and underload, repeated spike overloads every 1000 cycles, TWIST (Ref 26) and Mini-TWIST (Ref 27) loading. Using the closure model and some microstructural features, a total fatigue life prediction method is demonstrated on a titanium alloy under constant-amplitude loading and on several aluminum alloys under various load histories. The load histories considered were the FALSTAFF (Ref 28), Gaussian (Ref 29), TWIST (Ref 26) and Mini-TWIST (Ref 27). The crack configurations used in these analyses were through-crack configurations, such as center-crack and compact specimens, and three-dimensional crack configurations, such as a corner crack in a bar and a surface or corner crack at a semi-circular notch.

PLASTICITY-INDUCED CRACK-CLOSURE MODEL

The crack-closure model (Refs 16 and 30) was developed for a central through-crack in a finite-width specimen subjected to remote applied stress. The model was later extended to a through-crack emanating from a circular hole and applied to the growth of small cracks (Ref 15 and 31). The model was based on the Dugdale model (Ref 32), but modified to leave plastically deformed material in the wake of the crack. A schematic of the model is shown in Figure 2. Here a crack is growing from a hole in an elastic body (Region 1). At the maximum applied stress, S_{max}, the material in the plastic zone, ρ, (Region 2) carries the stress, $\alpha\sigma_0$. The constraint factor, α, accounts for the influence of stress state on tensile yielding at the crack front. The flow stress σ_0 is the average between the yield stress and ultimate tensile strength. For plane-stress conditions, α is equal to unity (original Dugdale model); and for simulated plane-strain conditions, α is equal to 3. Although the strip-yield model does not model the correct yield-zone pattern for plane-strain conditions, the model with a high

constraint factor is able to produce crack-surface displacements and crack-opening stresses quite similar to those calculated from an elastic-plastic finite-element analysis of crack growth and closure for a finite-thickness plate (see Ref 33). As the crack grows under cyclic loading, residual-plastic deformed material (Region 3) is left on the crack surfaces. During unloading, these surfaces contact each other at the minimum applied stress. The material in the plastic zone and along the contacting surfaces was assumed to yield at $-\sigma_0$. (In the original model, the contacting surfaces were assumed to reduce the effectiveness of the crack and reduce the constraint around the crack front. On the basis of three-dimensional finite-element analyses, however, this assumption may need to be studied further but this is beyond the scope of the present paper.) Using the contact stresses, the crack-opening stress is calculated. The crack-opening stress is the applied stress level S at which the crack surfaces are fully open and is denoted as S_0'. The model is able to predict crack-opening stresses as a function of crack length and load history. The crack-opening stress is then used to calculate the effective stress-intensity factor range, ΔK_{eff} (Ref 12). In turn, the crack-growth rate is calculated using a ΔK_{eff}-against-crack-growth-rate relation.

In conducting fatigue-crack growth analyses, the constraint factor α was used to elevate the flow stress at the crack tip to account for three-dimensional stress states. At present, the constraint factor is used as a fitting parameter to correlate crack-growth rate data against ΔK_{eff} under constant-amplitude loading for different stress ratios. However, tests conducted under single-spike overloads seem to be more sensitive to state-of-stress effects and may be a more appropriate test to determine the constraint factor.

Effective Stress-Intensity Factor Range

For most damage tolerance and durability analyses, the linear-elastic analyses have been found to be adequate. However, for high stress-intensity factors, proof testing, and low-cycle fatigue conditions, the linear-elastic analyses are inadequate and nonlinear crack-growth parameters are needed (see Ref 10). Herein, the linear-elastic effective stress-intensity factor range, developed by Elber (Ref 12), was used and is given by

$$\Delta K_{eff} = (S_{max} - S_0') \sqrt{\pi c}\ F_j \qquad (1)$$

where S_{max} is the maximum applied stress, S_o' is the crack-opening stress, and F_j is the usual boundary-correction factor.

Constraint Variations

As a crack grows in a finite-thickness body under cyclic loading (constant stress range), the plastic-zone size at the crack front increases. At low stress-intensity factor levels, plane-strain conditions should prevail but as the plastic-zone size becomes large compared to sheet thickness, a loss of constraint is expected. This constraint loss has been associated with the transition from flat-to-slant crack growth, as illustrated in Figure 3. Schijve (Ref 34) has shown that the transition occurs at nearly the same crack-growth rate over a wide range in stress ratios for an aluminum alloy. Later, Schijve (Ref 35), using Elber's crack-closure concept, proposed that the transition should be controlled by ΔK_{eff}. This observation has been used to help select the constraint-loss regime (see Ref 31).

In a related effort to study constraint variations using a three-dimensional, elastic-plastic, finite-element analysis, some results are included here to help resolve the constraint-loss issue (see Ref 36). The finite-element code, ZIP3D (Ref 37), was used to analyze center-crack-tension and bend specimens made of a material with an elastic-perfectly-plastic stress-strain behavior. The analyses were conducted on a 2.5 mm-thick sheet with various half-widths (w) and a c/w ratio of 0.5. The crack front was flat and straight-through the thickness. The finite-element model (one-eighth of the specimen) had six layers through the half-thickness with the layer on the centerline of the specimen being 0.15B and the layer on the free surface being 0.025B. The smallest element size around the crack front was about 0.03 mm. The number of elements was 5706 and the number of nodes was 7203. The finite-element model of the specimen was subjected to monotonic loading until the plastic zone extended across the net section.

Because the current model uses a constant flow stress in the plastic zone, a global constraint factor, α_g, was defined as the average of the normal stress to flow stress (σ_{yy}/σ_o) ratio in the plastic zone. Figure 4 shows a comparison of α_g as a function of the normalized applied K level for tension and bend specimens. The symbols show the results from the finite-element analyses for various specimen sizes. The upper dashed lines show the results under plane-strain conditions; the lower dashed line shows the

plane-stress condition. The global constraint factor was nearly a unique function of the applied K level. Some slight differences were observed near the plane-stress conditions (high K levels). These results show that the global constraint factor rapidly drops as the K level increases (plastic-zone size increases) and approaches a value near the plane-stress condition. The solid line is a simple fit to the finite-element results and shows that the constraint-loss regime may be defined by a unique set of K values under monotonic loading and, possibly, ΔK_{eff} under cyclic loading. In the current model, the constraint-loss regime is defined by a set of crack-growth rates because the transition from flat-to-slant crack growth seems to occur at unique rates. This assumption also implies that a unique set of ΔK_{eff} values define the constraint-loss regime.

Constant-Amplitude Loading

In Reference 38, crack-opening stress equations for constant-amplitude loading were developed from crack-closure model calculations for a center-crack tension specimen. These equations give crack opening stresses as a function of stress ratio (R), maximum stress level (S_{max}/σ_o) and the constraint factor (α). To correct the previous crack-opening stress equations for extremely high crack-growth rates, a modification was developed in Reference 17. The new equations give crack-opening stresses that agree fairly well with results from the modified closure model. These equations are used to develop the baseline ΔK_{eff}-rate relations that are used in the life-prediction code FASTRAN-II (Ref 39) to make crack-growth and fatigue-life predictions. A typical comparison between the model and the equations for a crack in a titanium alloy is shown in Figure 5. This figure shows crack-opening stresses as a function of crack length for a crack in an infinite plate at low R. To severely test the equations with a rapid change in constraint, α was selected to be 2.4 for rates less than 1E-04 mm/cycle; and α was 1.2 for rates greater than 1E-03 mm/cycle. The solid curve shows the calculations from the model. To use the crack-opening stress equations, the R ratio, the S_{max}/σ_o ratio and the constraint factor must be known a priori. In this example, the constraint factor is unknown as a function of crack length. Because rates are used to control the constraint factor in the model, the crack-growth rate must be known to calculate the crack-opening stress. The crack-length-against-cycles results

from the model were therefore used to determine the rate for a given crack length. Knowing the rate, then the constraint factor is calculated from

$$\alpha = \alpha_2 + (\alpha_1 - \alpha_2)[\log(dc/dN) - \log(r_2)]/[\log(r_1) - \log(r_2)] \qquad (2)$$

for $r_1 < dc/dN < r_2$ where α_1 and α_2 are the constraint factors, and r_1 and r_2 are the rates, at the beginning and end of the constraint-loss regime, respectively. For rates less than r_1, $\alpha = \alpha_1$ and for rates greater than r_2, $\alpha = \alpha_2$. Once the constraint factor has been determined, then the crack-opening stress is calculated from the equations (dashed curve). For constant α regions, the results from the equations agreed well with the model. Some differences were observed in the transition region between α = 2.4 to 1.2, but the maximum error in calculating ΔK_{eff} was only 4 percent. The small vertical lines indicate the corresponding life ratio (N/N_f), in addition to indicating regions of constant constraint.

Spectrum Loading

For variable-amplitude and spectrum loading, the crack-closure model must be used to compute the crack-opening stress history. Some typical crack-opening stresses under the Mini-TWIST load sequence for a small surface crack in a single-edge-notch-tension (SENT) specimen are shown in Figure 6. In the small-crack simulation, an initial defect size of a_i = 3 μm and c_i = 9 μm was used. This size corresponds to inclusion-particle sizes that initiate cracks in some aluminum alloys (Refs 7 and 8). Variable constraint was selected for this simulation. The constraint factor (α) was 1.8 for crack-growth rates less than 7E-04 mm/cycle and 1.2 for rates greater than 7E-03 mm/cycle. The figure shows crack-opening stress (normalized by the maximum stress in the spectrum) plotted against the ratio of applied cycles to cycles-to-failure (N/N_f). The predicted cycles to failure, N_f, was about 800,000 cycles. These results show that the opening stresses start near the minimum stress in the spectrum and rise as the crack grows. Crack-opening stresses tended to level off for N/N_f between 0.7 and 0.9. The rapid jump in S_0'/S_{max} for an N/N_f ratio of about 0.92 was caused by the change in constraint from 1.8 to 1.2 at the higher crack-growth rates. The surface crack became a through crack (a/t = 1) at an N/N_f ratio of about 0.9.

LARGE-CRACK GROWTH BEHAVIOR

To make life predictions, ΔK_{eff} as a function of the crack-growth rate must be obtained for the material of interest. Fatigue crack-growth rate data should be obtained over the widest possible range in rates (from threshold to fracture), especially if spectrum load predictions are required. Data obtained on the crack configuration of interest would be helpful but it is not essential. The use of the nonlinear crack-tip parameters is only necessary if severe loading (such as low cycle fatigue conditions) are of interest. Most damage-tolerant life calculations can be performed using the linear elastic stress-intensity factor analysis with crack-closure modifications.

Constant-Amplitude Loading

Under constant-amplitude loading, the only unknown in the analysis is the constraint factor, α. The constraint factor is determined by finding (by trial-and-error) an α value that will correlate the constant-amplitude fatigue-crack-growth-rate data over a wide range in stress ratios, as shown in References 30 and 38. This correlation should produce a unique relationship between ΔK_{eff} and crack-growth rate. In the large-crack-growth threshold regime for some materials, the plasticity-induced closure model may not be able to collapse the threshold (ΔK-rate) data onto a unique ΔK_{eff}-rate relation because of other forms of closure. Roughness- and oxide-induced closure (see Ref 40) appear to be more relevant in the threshold regime than plasticity-induced closure. This may help explain why the constraint factors needed to correlate crack-growth rate data in the near threshold regime, that is, plane-strain conditions, are 1.7 to 1.9 for aluminum alloys, 1.8 to 2 for titanium alloys and 2.5 for steel. However, further study is needed to assess the interactions between plasticity-, roughness- and oxide-induced closure in this regime. If the plasticity-induced closure model is not able to give a unique ΔK_{eff}-rate relation in the threshold regime, then high stress ratio ($R \geq 0.7$) data may be used to establish the ΔK_{eff}-rate relation.

In the following, the ΔK_{eff}-rate relations for one aluminum alloy and two titanium alloys will be presented and discussed. Similar procedures were used to establish the relationships for all materials used in this study. The large-crack results for 7075-T6 aluminum alloy are shown in Figure 7 for data generated at two different laboratories and at three

stress ratios (Ref 20). The data collapsed into a narrow band with several transitions in slope occurring at about the same rate for all stress ratios. Some differences were observed in the threshold regime. For these calculations, a constraint factor α of 1.8 (nearly equivalent to Irwin's plane-strain condition) was used for rates less than 7E-04 mm/cycle (start of transition from flat-to-slant crack growth) and α equal to 1.2 was used for rates greater than 7E-03 mm/cycle (end of transition from flat-to-slant crack growth). For intermediate rates, α was varied linearly with the logarithm of crack-growth rate. The values of α were selected by trial-and-error. The solid symbols (see upper left-hand portion of figure) denote measured rates at the end of transition from flat-to-slant crack growth (Refs 20 and 41). It has been proposed in Reference 31 that the flat-to-slant crack-growth transition region may be used to indicate a change from nearly plane-strain to plane-stress behavior and, consequently, a change in constraint. In the low crack-growth rate regime, near and at threshold, some tests (Ref 14) and analyses (Ref 15) have indicated that the threshold develops because of a rise in the crack-opening-stress-to-maximum-stress ratio due to the load-shedding procedure. In the threshold regime then, the actual ΔK_{eff}-rate data would lie at lower values of ΔK_{eff} because the rise in crack-opening stress was not accounted for in the current analysis. For the present study, an estimate was made for this behavior and it is shown by the solid line below rates of about 2.0E-6 mm/cycle. The baseline relation shown by the solid line will be used later to predict small-crack growth rates and fatigue lives under constant-amplitude loading.

Figure 8 shows the ΔK_{eff}-rate data for corner cracks in 10 mm-thick Ti-6Al-4V titanium alloy (Ref 23). In these tests, the initial defect size was a 250 μm-quarter-circular electrical-discharged machined notch. The data correlated quite well with a constant constraint factor of 1.9. For thick materials, the loss of constraint, as shown for the thin 7075-T6 alloy (Fig 7), may occur at higher values of ΔK_{eff} than those shown for the thinner material. Consequently, a constant constraint factor was used over the whole rate range. The solid symbols show the results of 13 mm-thick compact specimens (Ref 42) tested over a wide range of R ratios and down to much lower rates than the corner-crack tests. The baseline relation (solid line), fit to the corner-crack results in the mid-region and the compact results in the low-rate regime, will be used later to predict crack-growth rates for tests with spike overloads repeated every 1000 cycles.

The ΔK_{eff}-rate results for IMI-685 titanium alloy compact specimens (Refs 23 and 25) are shown in Figure 9. This material was selected to be analyzed because "roughness-induced" closure was expected to be prevalent. These data also illustrate two difficulties with correlating test data using the linear-elastic effective stress-intensity factor ranges and the plasticity-induced closure model. First, the high R ratio results tend to deviate from the low R ratio results near the end of the tests. These specimens were cycled to failure and the last few data points were taken immediately before the specimen failed. The maximum stress level for the high R ratio test was considerably higher than that used for the low R ratio test; and plasticity effects would have been greater in the high R test than the low R, resulting in higher rates for a given value of elastic ΔK_{eff}. However, fitting the ΔK_{eff} relation to the low R ratio results (solid line) will allow accurate life prediction for both the low and high R ratio conditions, because the high R ratio tests are predicted to fail at a ΔK_{eff} value of 23 MPa$\sqrt{m}$ (fracture toughness K_c = 80 MPa$\sqrt{m}$). Thus, accurately modelling the upper tail of the high R ratio test would not have greatly affected the number of cycles to failure. The second difficulty with the model occurs in the threshold regime and shows that threshold data (load-reduction tests) begin to form bands of data as a function of R, especially for materials where roughness-induced closure may occur. The steady-state crack-opening stress equations do not account for any load-reduction effects nor roughness-induced closure which is expected to be dominate in the IMI-685 alloy. Because cracks in the high R ratio tests are expected to be fully open, these results were used to determine the ΔK_{eff} relation at the low rates. The baseline relation will be used later to make crack growth predictions under repeated spike overloads.

Spike Overload and Underload

For variable-amplitude or spectrum load crack-growth predictions, the constraint factor should also be verified by some simple tests, such as crack growth after a single-spike overload. Constraint factors appear to be more sensitive to crack-growth delays caused by single-spike overloads than to crack growth under constant-amplitude loading at different stress ratios. Higher values of α will cause less load-interaction effects, such as retardation or acceleration, than lower values of constraint. Thus, spike-

overload tests may be more useful in establishing values of α than constant-amplitude tests. However, the constraint factors determined by spike-overload tests should also correlate constant-amplitude data (see Ref 43).

A comparison of measured and predicted rates for large cracks after a single spike overload and after a single spike overload followed by an underload are shown in Figure 10. Cracks were grown under constant-amplitude loading (R = 0.4 with K_{max} = 19.7 MPa$\sqrt{m}$) to a crack length of 12 mm. In one case, a single overload, K_{OL} = 31.4 MPa$\sqrt{m}$, was applied and then the test was returned to constant-amplitude loading. The second case was identical to the first case, except that an underload K_{UL} = -3.9 MPa$\sqrt{m}$ was applied immediately after the overload. Two methods were used to measure crack length and rates in the 7475 alloy (Ref 22): the direct-current potential method (solid symbols) and the scanning-electron microscope (open symbols). The predicted results using the closure model with α = 1.9 (curves) agreed well with the test results, especially for the overload-underload case. For the overload case, the experimental rates did not appear to stabilize at the pre-overload rates as quickly as the predictions. These results indicate that the constraint factor of 1.9 is appropriate for these conditions. But overloads at higher K_{OL} values would be expected to cause some loss of constraint (lower α). Under these conditions, the analyses using an α = 1.9 would be expected to predict higher rates and less retardation than the tests. Thus, variable constraint may be needed to predict the behavior.

Repeated Spike Overloads

Figures 11 and 12 show measured and predicted ΔK-rate results for repeated spike overloads applied to compact and corner-crack specimens made of IMI-685 and Ti-17 titanium alloys, respectively. These tests were conducted under constant-amplitude loading (R = 0.1) with an overload (P_{OL} = 1.7 P_{max}) applied every 1,000 cycles (Refs 23 and 24). The overall trends in the predicted results for the IMI-685 corner-crack configuration agreed well with the test results at low rates. However, the predicted rates tended to be somewhat high in the middle and upper ranges. Although the predicted results for the compact specimen agreed fairly well with the test data, the test results on each individual specimen were not modelled very accurately. The measured rates on one of the compact specimens in the beginning of the test were much lower than predicted. The oscillating

behavior in the predicted results at high rates was caused by averaging rates over less than 1000 cycles, thus accelerations and retardations during and after the spike overload are being shown. The comparison of measured and predicted rates on the Ti-17 alloy agreed quite well (Fig 12). A comparison of predicted-to-test lives (N_p/N_t) for these titanium alloys and Ti-6Al-4V, for the two crack configurations, ranged from 0.57 to 2.12 but most results were within about 20 percent of the test results. These results are presented and discussed in Reference 24.

Spectrum Loading

Wanhill (Ref 18) conducted spectrum crack-growth tests on center-crack tension specimens made of 2024-T3 Alclad material in two thicknesses (B = 1.6 and 3.1 mm). Tests were conducted under the TWIST spectrum clipped at Levels I and III with S_{mf}= 70 MPa. The initial crack starter notch half-length was 3.5 mm. Comparisons are made between experimental and calculated crack length against flights for Level III; and experimental and calculated crack length against crack-growth rate for Levels I and III.

Crack-length-against-flight data on the 3.1 mm-thick specimens tested under the TWIST (Level III) loading are shown in Figure 13. The solid curve is the calculated results from the closure model with the variable-constraint condition (α = 2 to 1) using the baseline ΔK_{eff}-rate relation and constraint-loss regime established in Reference 44. To illustrate why the variable-constraint conditions are necessary, example calculations were made for constant constraint conditions of either α = 1 or 2 (dashed-dot curves). The model with a low constraint condition (α = 1) predicted much longer flights to a given crack length than the test data. Conversely, the predicted results for the higher constraint condition (α = 2) greatly under predicted the behavior except in the early stages of growth. Thus, the placement of the constraint-loss regime is crucial to making accurate crack-growth predictions under aircraft spectrum loading.

Figure 14 shows a comparison between experimental (Ref 18) and calculated results of crack length against dc/dF under the TWIST loading (Levels I and III) for the 1.6 mm-thick specimens. The crack-growth rate, dc/dF, is the change in crack length per flight. For both levels, the closure model was able to calculate the initial rates quite accurately (curves). Calculated results under Level III agreed with the test results

over nearly the complete range of crack lengths. The calculated results under Level I, however, began to deviate from the test results after a crack length of about 12 mm. The ratio of calculated life to test life from an initial crack length of 3.5 mm to failure was 0.61 for Level I.

SMALL-CRACK GROWTH BEHAVIOR

In the following, comparisons are made between measured and predicted crack-shape changes and crack-growth rates for small surface cracks at a notch in 7075-T6 aluminum alloy under constant-amplitude loading. Comparisons are also presented on measured and predicted rates for small corner cracks at a notch in LC9cs clad aluminum alloy under both constant-amplitude and Mini-TWIST spectrum loading. The plastic-replica method was used to measure the initiation and growth of the small cracks and these results are presented and discussed in Reference 20.

Figure 15 shows the crack-depth-to-crack-length (a/c) ratio plotted against the crack-depth-to-sheet-half-thickness (a/t) ratio for the 7075-T6 alloy. Measured a/c and a/t ratios (open symbols) were determined from an experimental method where specimens were broken at various stages during their life. Results are shown for three stress ratios and for the Mini-TWIST spectrum loading. The spectrum has an overall stress ratio (minimum to maximum stress in the spectrum) of -0.23. The solid symbols show the sizes and shapes of inclusion-particle clusters or voids which initiated cracks (average size was a_i = 3 μm and c_i = 9 μm).

The curves in Figure 15 show the predictions for the different stress ratios using the average inclusion-particle cluster size. In the analyses, the crack-growth rate relations for da/dN was different than that for dc/dN as a function of ΔK_{eff} (see Ref 20). The tests and analyses show that small surface cracks tend to rapidly approach an a/c ratio of about unity for a large part of their growth through the thickness.

Comparisons of experimental and predicted crack-growth rates for small cracks under R = -1 loading are shown in Figures 16 and 17 for 7075-T6 and LC9cs alloys, respectively. For the 7075-T6 alloy, small surface cracks initiated along the notch surface from inclusion-particle clusters or voids. For the LC9cs alloy, small corner cracks initiated in the cladding layer from slip-band formation (cladding thickness was 50 to 70 μm). Even though the range in maximum stress levels used in each test series are indicated on the figures, no stress-level effect was apparent in the test data and all

data have been grouped together. However, a range in stress levels was used in the analyses to show some expected trends with stress level. The dash-dot line show the large crack (dc/dN) results and the dashed line show the ΔK_{eff}-rate curve used in the analyses for da/dN. The solid curves show the predicted results using an initial defect size (3 by 9 by 0.5 μm for 7075-T6; and 77 by 77 by 0.5 μm for LC9cs). All predictions start on the ΔK_{eff} curve because cracks at small voids were assumed to be fully open on the first cycle and ΔK is equal to ΔK_{eff}. For the 7075-T6 alloy (Fig 16), the predictions from the model did not agree very well with the test data for S_{max} = 80 to 95 MPa in the near threshold regime. In Reference 20, part of this discrepancy was attributed to an influence of the acetone used in taking plastic replicas of the notch surface. Fatigue lives for specimens with replicas were much longer (about a factor of 4) than those without replicas. However, the predictions did agree with the test data in the mid- and high-rate range. At 70 MPa, the predictions show that the crack would be nearly arrested (minimum rate) at a ΔK-value of about 2 MPa$\sqrt{m}$. At this point the ΔK_{eff} was slightly greater than 0.9 MPa$\sqrt{m}$, the effective threshold for small cracks. (Note that the endurance limit for R = -1 was about 70 MPa, see Reference 20.)

For the LC9cs alloy (Fig 17), the predictions from the model agreed well with the test data for S_{max} = 70 to 90 MPa in the early stages of crack growth. The predicted rates seem to be slightly low in the mid- to high-rate range. At 50 MPa, the predictions show a large drop in the crack-growth rates, similar to the 7075-T6 alloy. The crack would have been predicted to arrest if an applied stress of 40 MPa had been used. Again, the effective threshold for small cracks was assumed to be 0.9 MPa$\sqrt{m}$ and the endurance limit was about 40 MPa.

The measured and predicted small-crack growth rates for the Mini-TWIST loading are shown in Figures 18 for the LC9cs alloy. Here the "average" crack-growth rate is plotted against the "maximum range" stress-intensity factor. The average crack-growth rate is the change in crack length per replica interval (about 30,000 cycles) and the stress-intensity factor range is computed using the maximum and minimum stress levels in the Mini-TWIST spectrum. The predicted values were determined in the following way. Crack length (2a) and cycle results were taken from the analysis at nearly equal cyclic intervals between the initial crack length and breakthrough (a = t). From these values of crack length and cycles, the average rate and maximum

range stress-intensity factor were calculated. The predicted rates (solid curve) agreed well with the experimental data for both small- and large-crack behavior.

FATIGUE-LIFE PREDICTIONS

At this point, all of the elements are in place to assess a total fatigue-life prediction methodology based solely on crack propagation from microstructural features. In this approach, a crack is assumed to initiate and grow from a microstructural feature on the first cycle. The crack-closure model and the baseline ΔK_{eff}-rate curves are used to predict crack growth from the initial crack size to failure. Comparisons are made with fatigue tests conducted on the single- or double-edge-notch tension specimens. Results are presented for three aluminum alloys and one titanium alloy under either constant-amplitude or various spectrum loadings.

Constant-Amplitude Loading

Fatigue life (S-N) data for 7075-T6 aluminum alloy are shown in Figure 19 for constant-amplitude loading. A symbol indicates a failure and a symbol with an arrow indicates that a test was terminated before failure. In the analysis, the initial crack size was a_i = 3 μm, c_i = 9 μm and b = 0.5 μm (defect or void half-height). This crack size is the average inclusion-particle or void size that was measured at actual crack-initiation sites. The effective stress-intensity factor range against rate relation used in the analysis is given in Reference 20 and $(\Delta K_{eff})_{th}$ was assumed to be 0.9 MPa$\sqrt{m}$. Using the life-prediction code (Ref 39), predictions were made for constant-amplitude loading. The solid curves show the predicted number of cycles to failure. The predicted lives were in reasonable agreement with the test lives. In addition to predicting fatigue life, the analysis methodology was also able to fit the endurance limit as a function of stress ratio.

Fatigue tests were conducted on Ti-6Al-4V titanium alloy double-edge-notch tension (DENT) specimens in the AGARD Engine Disc Cooperative Test Programme (Ref 24). These results (symbols) are shown in Figure 20 for two fan disc forgings. To make fatigue life calculations, the baseline ΔK_{eff}-rate relation, shown in Figure 8, was used to calculate the life of the titanium specimens. Because no information on crack-initiation behavior was given in Reference 24, life calculations were made on initial crack sizes

that would bound the experimental data, like the equivalent-initial-flaw size (EIFS) concept (Ref 46). The solid curves show the calculations for an initial semi-circular surface crack of a_i = 5 and 25 μm at the notch root. The solid symbol on the stress axis denotes where the net-section stress is equal to the ultimate tensile strength. Because of the notch configuration, notch strengthening is expected and the upper plateau is an estimate for the maximum net-section stress based on the results from the finite-element analyses (see Fig 4 at the high K levels). In a microstructural analysis, Wanhill and Looije (Ref 45) found that the primary α grains were about 10 μm in diameter and the transformed and aged β grains were about 20 μm in diameter for these fan disc materials. Further study is needed on these materials to see if cracks of these sizes would be present early in life or to see if the baseline curve (Fig 8) is appropriate for small cracks. For low ΔK_{eff} values, small cracks in the titanium alloys may grow faster than large cracks, as observed by Lanciotti and Galatolo (Ref 47).

Spectrum Loading

Experimental and predicted results for fatigue tests conducted on 7075-T6 bare and LC9cs clad alloy specimens under the Mini-TWIST spectrum are shown in Figure 21. These tests were conducted on SENT specimens (Ref 20). The solid and dashed curves show predictions for each alloy using the initial defect sizes shown. The defect size for 7075-T6 was the average inclusion-particle size that initiated cracks, whereas the initial crack size for the clad alloy LC9cs was somewhat larger than the cladding-layer thickness (50 to 70 μm). The predicted lives were in reasonable agreement with the test results (symbols) but the predicted lives tended to fall on the lower bound of the test data.

Comparisons of experimental and predicted fatigue lives of notched 2024-T3 aluminum alloy sheet specimens under FALSTAFF, Gaussian and TWIST load sequences are shown in Figure 22. These tests were conducted on SENT specimens (Refs 7 and 19) but they were cycled until a crack had grown across the full sheet thickness instead of failure. The predictions were made using an initial crack size that was the average inclusion-particle size that initiated cracks. The predicted lives agreed well with the test data.

CONCLUDING REMARKS

The "plasticity-induced" crack-closure model was used to correlate large-crack data on several aluminum and titanium alloys under constant-amplitude loading. A constraint factor, which accounts for three-dimensional state-of-stress effects, was used in determining the effective stress-intensity factor range against rate relations. These relations were then used to predict large-crack growth under variable-amplitude and spectrum loading. Comparisons made between measured and predicted small-crack growth rates in two aluminum alloys showed that the closure model could predict the trends that were observed in the tests. Using the closure model and some microstructural features, such as inclusion-particle sizes and cladding-layer thickness, a total fatigue-life prediction method was demonstrated. Fatigue life of notched specimens made of three aluminum alloys were compared with predicted lives under either constant-amplitude or spectrum loading. The predicted results were well within a factor of two of the test data. Fatigue lives for Ti-6Al-4V titanium alloy could also be bounded by using initial crack sizes of 5 and 25 μm in the life-prediction method.

Further study is needed to determine constraint variations along fatigue crack fronts in various materials and thicknesses. These constraint variations are needed to improve life predictions under aircraft spectrum loading, especially for thin-sheet materials. At low rates, the development of the large-crack threshold and its significance for design life calculations also needs further study.

REFERENCES

1. Gallagher, J. P.; Giessler, F. J.; Berens, A. P. and Engle, R. M., Jr., "USAF Damage Tolerant Design Handbook: Guidelines for the Analysis and Design of Damage Tolerant Aircraft Structures", AFWAL-TR-82-3073, May 1984.

2. Manning, S. D. and Yang, J. N., "USAF Durability Design Handbook: Guidelines for the Analysis and Design Aircraft Structures", AFWAL TR-83-3027, January 1984.

3. Small Fatigue Cracks, R. O. Ritchie and J. Lankford, eds., The Metallurgical Society, Inc., Warrendale, PA, 1986.

4. The Behaviour of Short Fatigue Cracks, K. J. Miller and E. R. de los Rios, eds., European Group on Fracture, Publication No. 1, 1986.

5. Rao, K. T. V. and Ritchie, R. O., "Fatigue of Aluminum-Lithium Alloys, Lawrence Berkeley Laboratory", LBL-30176, January 1991.

6. Behaviour of Short Cracks in Airframe Components, H. Zocher, ed., AGARD CP-328, 1983.

7. Newman, J. C. Jr. and Edwards, P. R., "Short-Crack Growth Behaviour in an Aluminum Alloy - an AGARD Cooperative Test Programme", AGARD R-732, 1988.

8. Short-Crack Growth Behavior in Various Aircraft Materials, P. R. Edwards and J. C. Newman, Jr., eds., AGARD Report No. 767, 1990.

9. El Haddad, M. H.; Dowling, N. E.; Topper, T. H. and Smith, K. N., "J Integral Application for Short Fatigue Cracks at Notches", International Journal of Fracture, Vol. 16, No. 1, 1980, pp. 15-30.

10. Newman, J. C., Jr., "Fracture Mechanics Parameters for Small Fatigue Cracks", Small Crack Test Methods, ASTM STP 1149, J. Allison and J. Larsen, eds., 1992, pp. 6-28.

11. Leis, B. N.; Kanninen, M. F.; Hopper, A. T.; Ahmad, J. and Broek, D., "Critical Review of the Short Crack Problem in Fatigue", Engineering Fracture Mechanics, Vol. 23, 1986, pp. 883-898.

12. Elber, W., "The Significance of Fatigue Crack Closure", Damage Tolerance in Aircraft Structures, ASTM STP 486, 1971, pp. 230-242.

13. Nisitani, H. and Takao, K. I., "Significance of Initiation, Propagation and Closure of Microcracks in High Cycle Fatigue of Ductile Materials", Engineering Fracture Mechanics, Vol. 15, No. 3-4, 1981, pp. 455-456.

14. Minakawa, K. and McEvily, A. J., "On Near-Threshold Fatigue Crack Growth in Steels and Aluminum Alloys", Proceedings of the International Conference on Fatigue Thresholds, Vol. 2, 1981, pp. 373-390.

15. Newman, J. C., Jr., "A Nonlinear Fracture Mechanics Approach to the Growth of Small Cracks", Behaviour of Short Cracks in Airframe Components, AGARD CP-328, 1983, pp. 6.1-6.26.

16. Newman, J. C., Jr., "A Crack-Closure Model for Predicting Fatigue Crack Growth under Aircraft Spectrum Loading", Methods and Models for Predicting Fatigue Crack Growth under Random Loading, J. B. Chang and C. M. Hudson, eds., ASTM STP 748, 1981, pp. 53-84.

17. Newman, J. C., Jr., Poe, C. C., Jr. and Dawicke, D. S., "Proof Test and Fatigue Crack Growth Modeling on 2024-T3 Aluminum Alloy", Fourth International Conference on Fatigue and Fatigue Thresholds, 1990, pp. 2407-2416.

18. Wanhill, R. J. H., "Flight Simulation Fatigue Crack Propagation Evaluation of Candidate Lower Wing Skin Materials with Particular Consideration of Spectrum Truncation", NLR TR 77092 U, July 1977.

19. Blom, A. F., "Short Crack Growth under Realistic Flight Loading: Model Predictions and Experimental Results for AL 2024 and AL-LI 2090", Short-Crack Growth Behavior in Various Aircraft Materials, P. R. Edwards and J. C. Newman, Jr., eds., AGARD Report No. 767, 1990, pp. 6.1-6.15.

20. Newman, J. C., Jr.; Wu, X. R.; Swain, M. H.; Zhao, W.; Phillips, E. P. and Ding, C. F., "Small-Crack Growth Behavior in High-Strength Aluminum Alloys - A NASA/CAE Cooperative Program", 18th Congress International Council of the Aeronautical Sciences, Sept. 20-25, 1992, ICAS-92-5.4.3.

21. Zhang, S.; Marissen, R.; Schulte, K.; Trautmann, K. -H.; Nowak, H. and Schijve, J., "Crack Propagation Studies on Al 7475 on the Basis of Constant Amplitude and Selective Variable Amplitude Loading Histories", Fatigue and Fracture of Engineering Materials and Structures, Vol. 10, 1987, pp. 315-332.

22. Zhang, S.; Doker, H.; Nowak, H.; Schulte, K. and Trautmann, K. H., "Improvements of Crack Propagation Analysis by More Exact Determination of K_{op}-Levels", Second Symposium on Fatigue Lifetime Predictive Techniques, ASTM, Pittsburgh, PA., 1992.

23. Raizenne, M. D., "AGARD SMP Sub-Committee 33 Engine Disc Test Programme Fatigue Crack Growth Rate Data and Modeling Cases for Ti-6Al-4V, IMI-685 and Ti-17", LTR-ST-1785, National Research Council Canada, Nov. 1990.

24. AGARD Engine Disc Cooperative Test Programme, Mom, A. J. A. and Raizenne, M. D., eds., AGARD Report No. 766, 1988; Pardessus, T., Jany, E. and Raizenne, M. D., eds., AGARD Report No. 766 (Addendum), 1993.

25. Hicks, M. A.; Jeal, R. H. and Beevers, C. J., "Slow Fatigue Crack Growth and Threshold Behaviour in IMI 685", Fatigue and Fracture of Engineering Materials and Structures, Vol. 6, No. 1, 1983, pp. 51-65.

26. deJonge, J. B.; Schutz, D.; Lowak, H. and Schijve, J., "A Standardized Load Sequence for Flight Simulation Tests on Transport Aircraft Wing Structures (TWIST)", NLR TR-73029 U, Nationaal Lucht-en Ruimtevaart-laborium, 1973.

27. Lowak, H.; deJonge, J. B.; Franz, J. and Schutz, D., "Mini-TWIST--A Shortened Version of TWIST", LBF Report No. TB-146, Laboratorium fur Betriebsfestigkeit, 1979.

28. van Dijk, G. M. and deJonge, J. B., "Introduction to a Fighter Loading Standard for Fatigue Evaluation--FALSTAFF", NLR MP 75017 U, Nationaal Lucht-en Ruimtevaartlaborium, May 1975.

29. Huck, M.; Schutz, W.; Fischer, R. and Kobler, H. G., "A Standard Random Load Sequence of Gaussian Type Recommended for General Application in Fatigue Testing", IABG Report No. TF-570 or LBF Report No. 2909, 1976.

30. Newman, J. C., Jr., "Prediction of Fatigue-Crack Growth under Variable-Amplitude and Spectrum Loading using a Closure Model", Design of Fatigue and Fracture Resistant Structures, P. R. Abelkis and C. M. Hudson, eds., ASTM STP 761, 1982, pp. 255-277.

31. Newman, J. C.; Swain, M. H. and Phillips, E. P., "An Assessment of the Small-Crack Effect for 2024-T3", Small Fatigue Cracks, Ritchie, R.O. and Lankford, J., eds., 1986, pp.427-452.

32. Dugdale, D. S., "Yielding of Steel Sheets Containing Slits, Journal of Mechanics and Physics of Solids", Vol. 8, Vol. 2, 1960, pp. 100-104.

33. Blom, A. F., Wang, G. S. and Chermahini, R. G., "Comparison of Crack Closure Results Obtained by 3-D Elastic-Plastic FEM and Modified Dugdale Model", Proceedings 1st International Conference on Computer Aided Assessment and Control of Localized Damage, Portsmouth, England, June 26-28, 1990, pp. 57-68.

34. Schijve, J., "Significance of Fatigue Cracks in Micro-Range and Macro-Range," Fatigue Crack Propagation, ASTM STP 415, 1967, pp. 415-459.

35. Schijve, J., "Shear Lips on Fatigue Fractures in Aluminum Alloy Sheet Material," Delft University of Technology, Report LR-287, Sept. 1979.

36. Newman, J. C., Jr., Bigelow, C. A. and Shivakumar, K. N., "Three-Dimensional Elastic-Plastic Finite-Element Analyses of Constraint Variations in Cracked Bodies", Engineering Fracture Mechanics, Vol. 46, No. 1, 1993, pp. 1-13.

37. Shivakumar, K. N. and Newman, J. C., Jr., "ZIP3D - An Elastic and Elastic-Plastic Finite-Element Analysis Program for Cracked Bodies," NASA TM 102753, Nov. 1990.

38. Newman, J. C., Jr., "A Crack-Opening Stress Equation for Fatigue Crack Growth", International Journal of Fracture, Vol. 24, 1984, R131-R135.

39. Newman, J. C., Jr., "FASTRAN II - A Fatigue Crack Growth Structural Analysis Program", NASA TM 104159, February 1992.

40. Ritchie, R. O. and Yu, W., "Short Crack Effects in Fatigue: A Consequence of Crack Tip Shielding", Small Fatigue Cracks, R. O. Ritchie and J. Lankford, eds., 1986, pp. 167-189.

41. Vogelesang, L. B., The Effect of Environment on the Transition from Tensile Mode to Shear Mode during Fatigue Crack Growth in Aluminum Alloys, Delft Report LR-286, Delft University of Technology, 1979.

42. Powell, B. E. and Henderson, I., "The Conjoint Action of High and Low Cycle Fatigue, AFWAL-TR-83-4119, Nov. 1983.

43. Newman, J. C., Jr. and Dawicke, D. S., "Prediction of Fatigue-Crack Growth in High-Strength Aluminum Alloy under Variable-Amplitude Loading", Advances in Fracture Research, K. Salama, K. Ravi-Chandar, D. M. R. Taplin and P. R. Rao, eds., Vol. 2, 1989, pp. 945-952.

44. Newman, J. C., Jr., "Effects of Constraint on Crack Growth under Aircraft Spectrum Loading", Fatigue of Aircraft Materials, A. Beukers, Th. de Jong, J. Sinke, A. Vlot and L. B. Vogelesang, eds., Delft University Press, 1992, pp. 83-109.

45. Rudd, J. L., Yang, J. N., Manning, S. D. and Garver, W. R., "Durability Design Requirements and Analysis for Metallic Airframes", Design of Fatigue and Fracture Resistant Structures, ASTM STP 761, P. R. Abelkis and C. M. Hudson, eds., 1982, pp. 133-151.

46. Wanhill, R. J. H. and Looije, C. E. W., "Fractographic and Microstructural Analysis of Fatigue Crack Growth in Ti-6Al-4V Fan Disc Forgings", AGARD Engine Disc Cooperative Test Programme, AGARD Report 766 (addendum), 1993.

47. Lanciotti, A. and Galatolo, R., "Short Crack Observations in Ti-6Al-4V under Constant-Amplitude Loading", Short-Crack Growth Behaviour in Various Aircraft Materials, P. R. Edwards and J. C. Newman, Jr., eds., AGARD R-767, 1990, pp. 10.1-10.7.

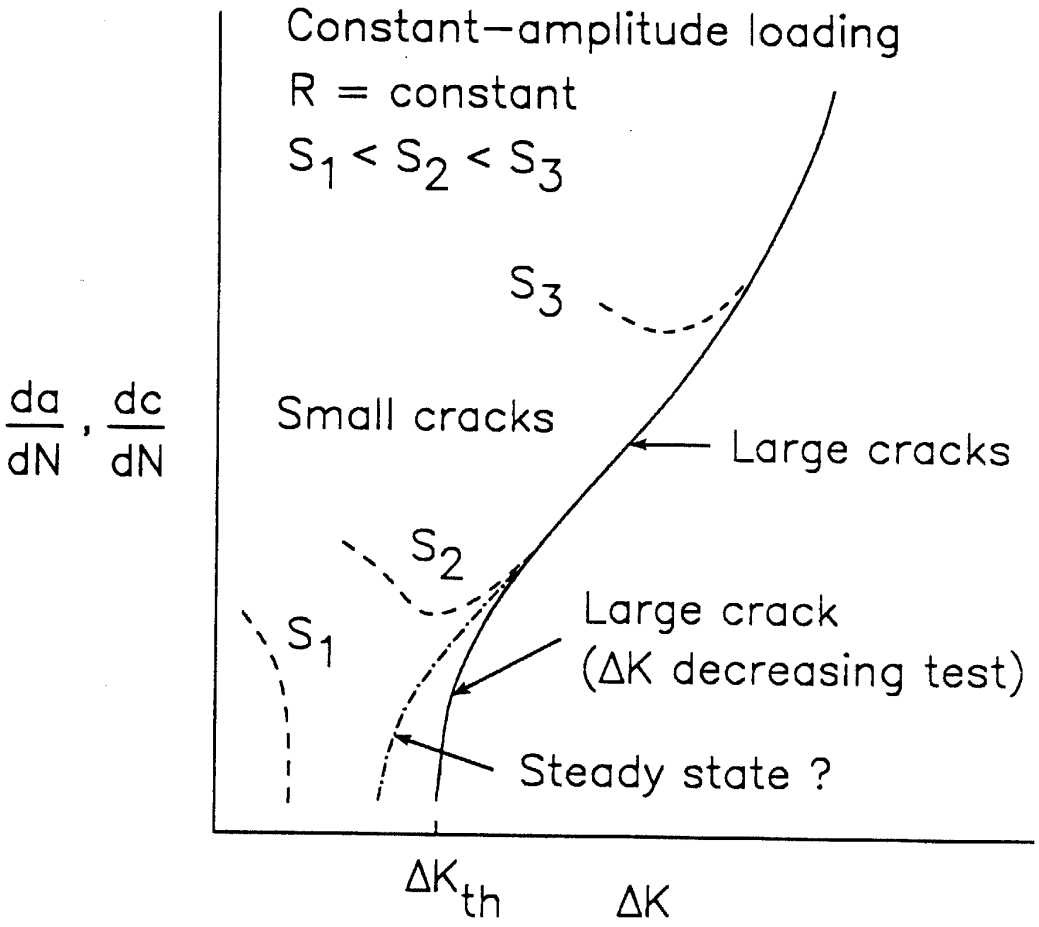

Fig. 1 Typical fatigue-crack-growth rate data for small and large cracks.

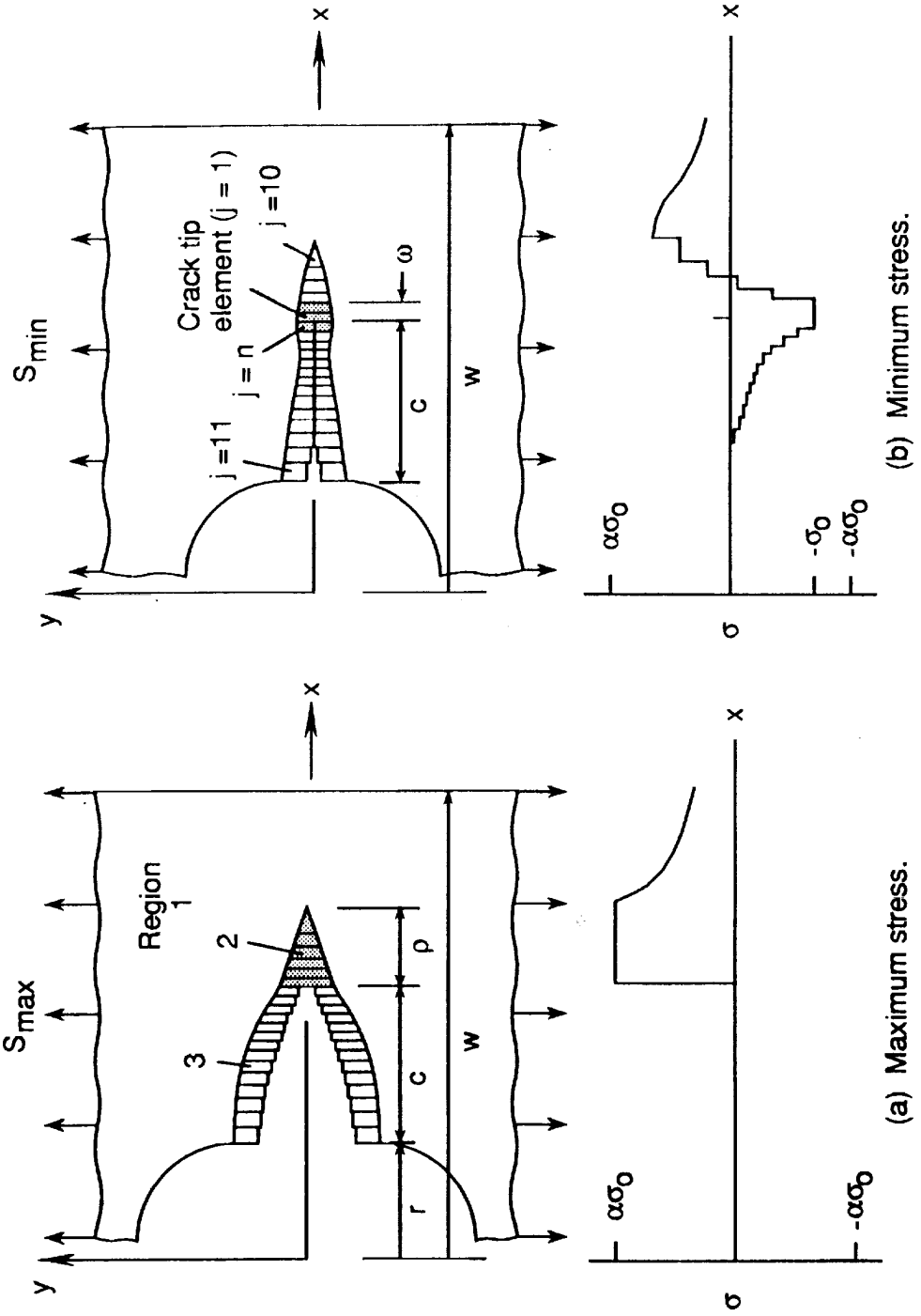

Fig. 2 Schematic of crack-closure model under cyclic loading.

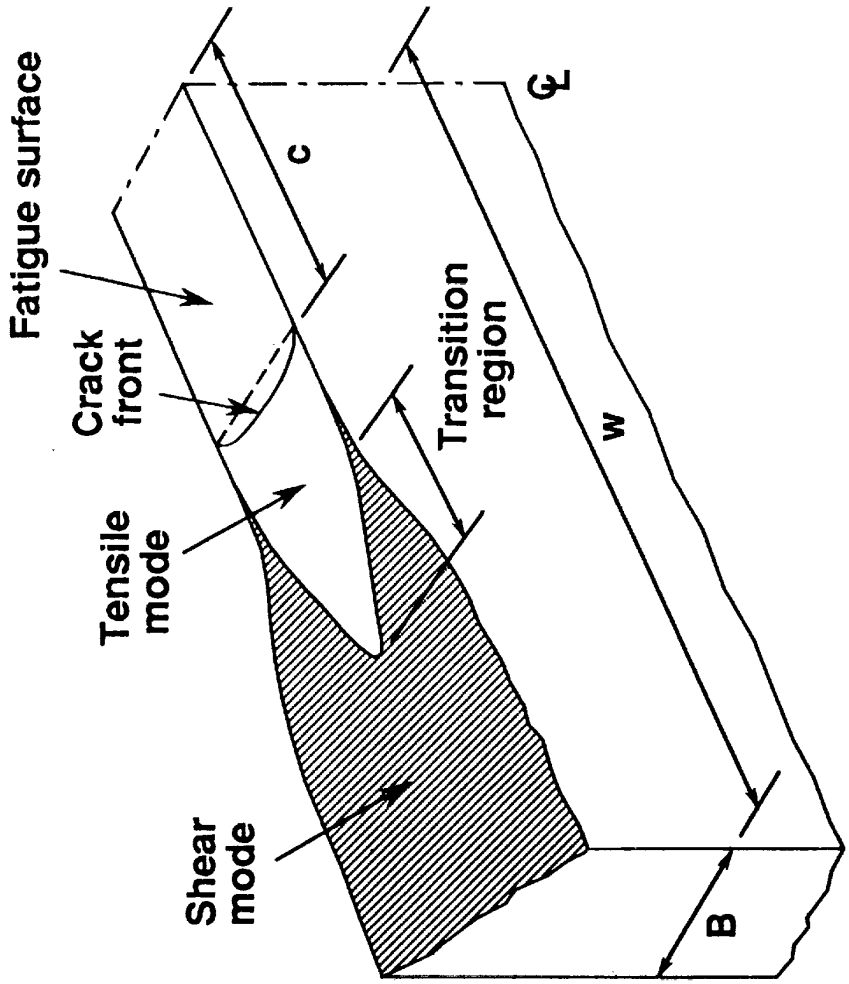

Fig. 3 Fatigue crack surface with transition from tensile to shear mode.

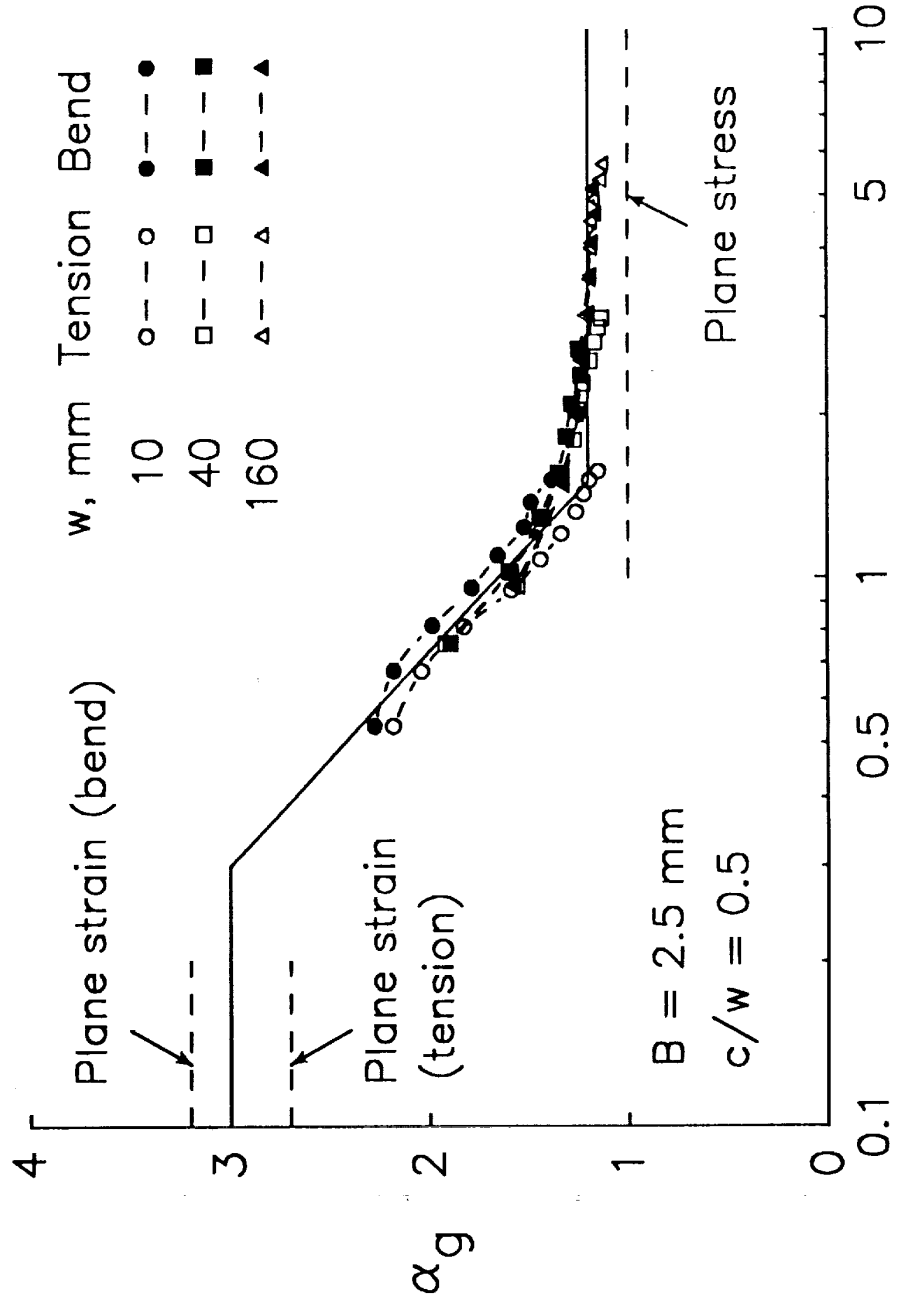

Fig. 4 Global constraint factor from 3D finite-element analyses for various size tension and bend specimens made of a thin sheet material.

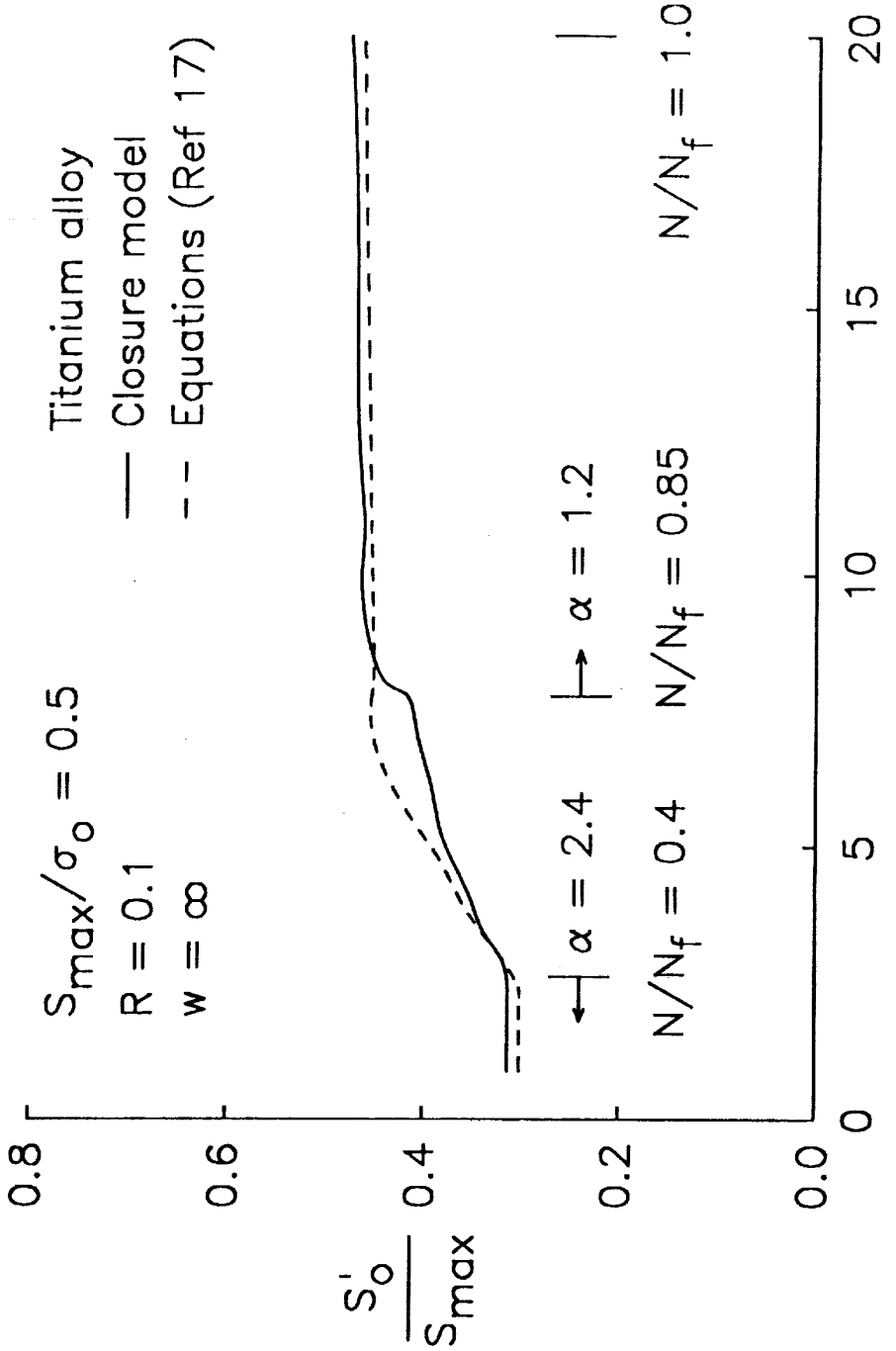

Fig. 5 Calculated crack-opening stresses from model and equations during regions of constant and changing constraint.

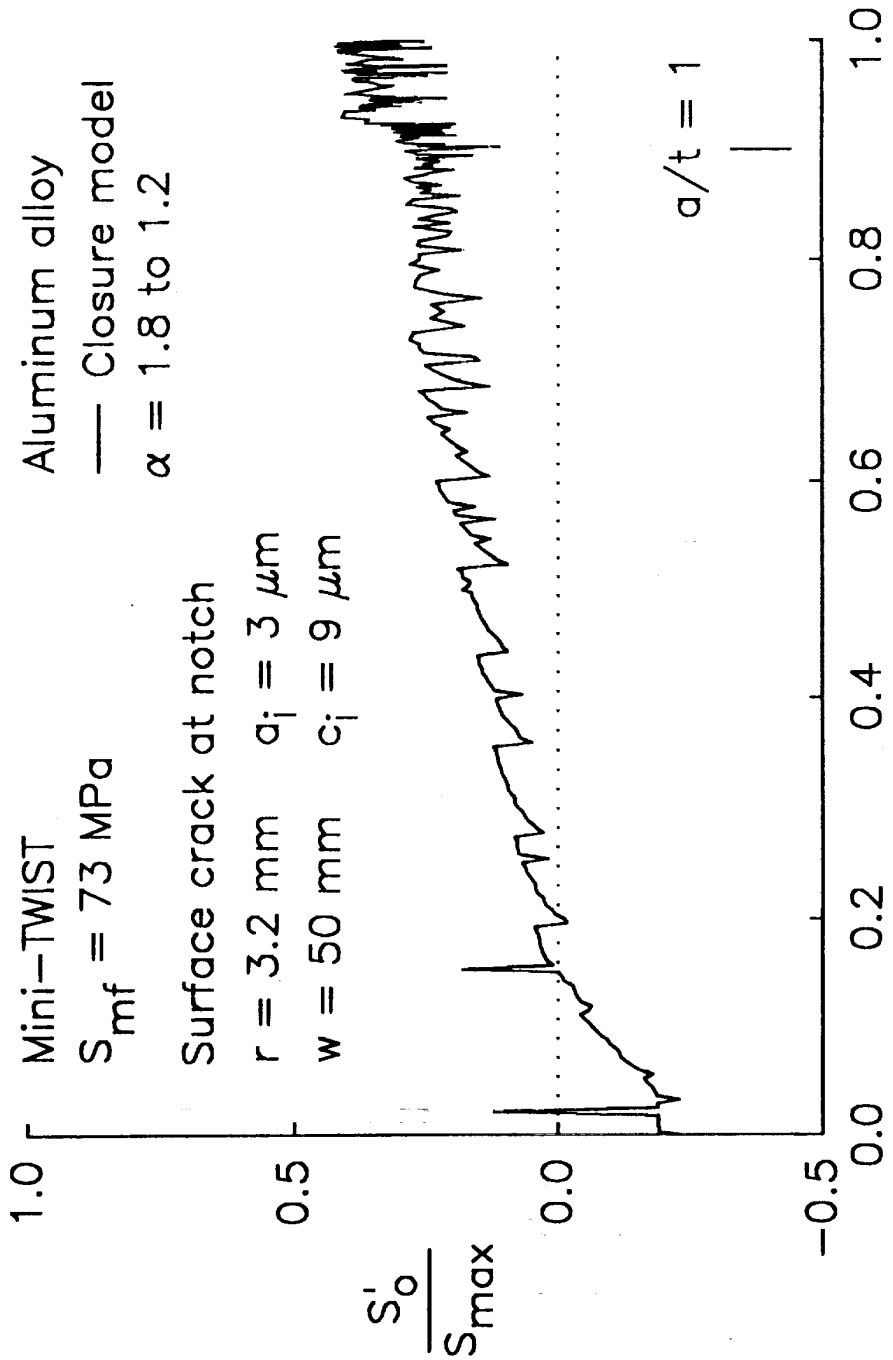

Fig. 6 Calculated crack-opening stresses for a small surface crack in an aluminum alloy under Mini-TWIST spectrum loading.

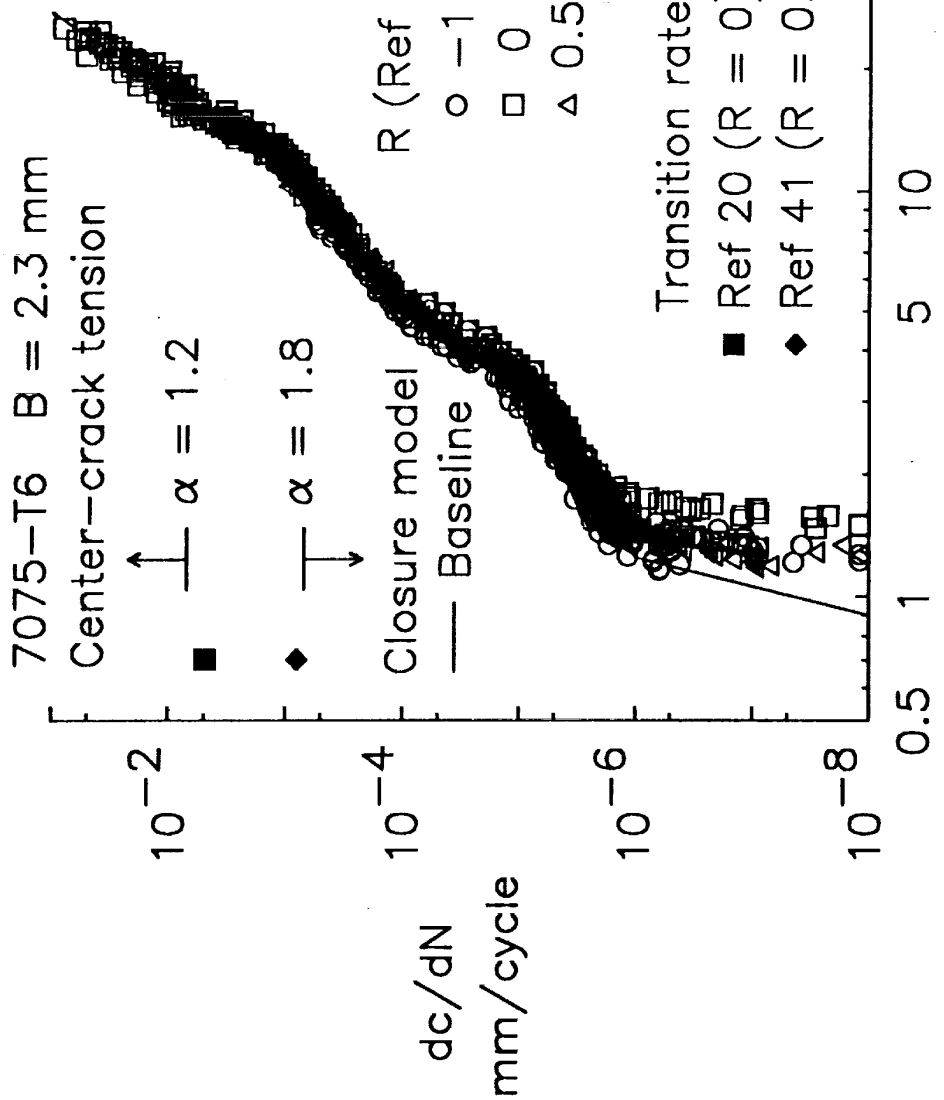

Fig. 7 Effective stress-intensity factor range against crack-growth rate for large cracks in 7075-T6 aluminum alloy.

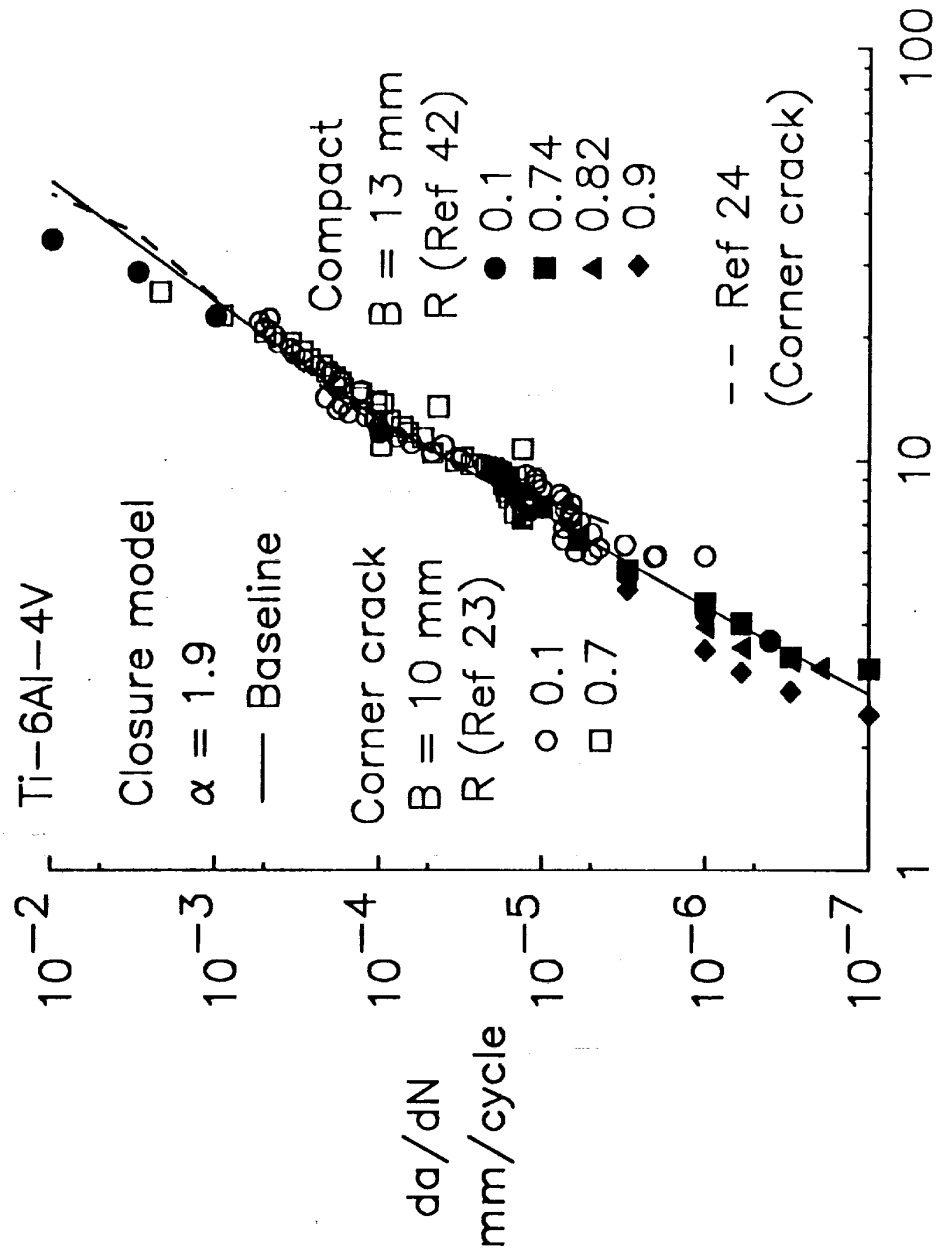

Fig. 8 Effective stress-intensity factor range against crack-growth rate in Ti-6Al-4V titanium alloy corner-crack and compact specimens.

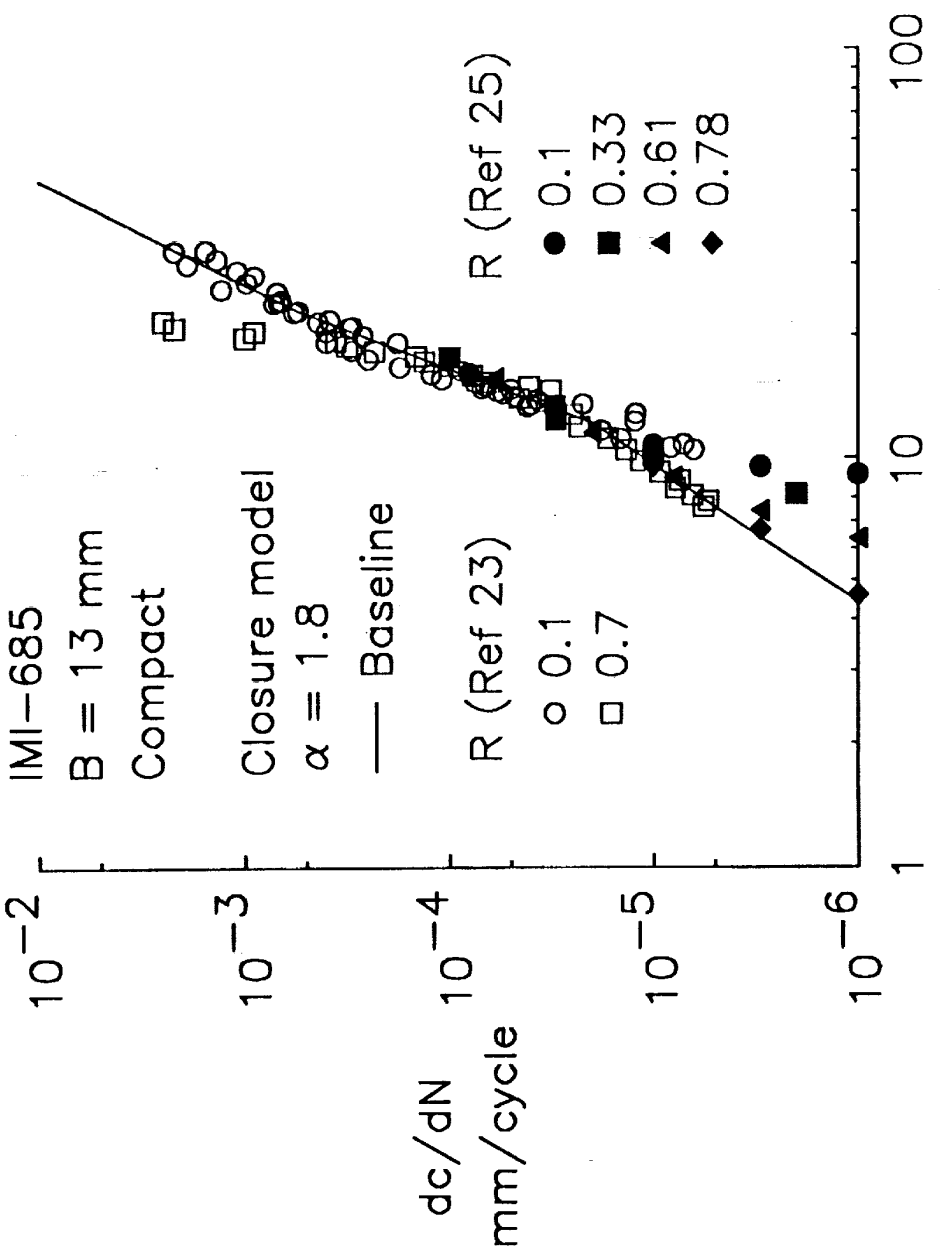

Fig. 9 Effective stress-intensity factor range against growth rate for large cracks in IMI-685 titanium alloy compact specimens.

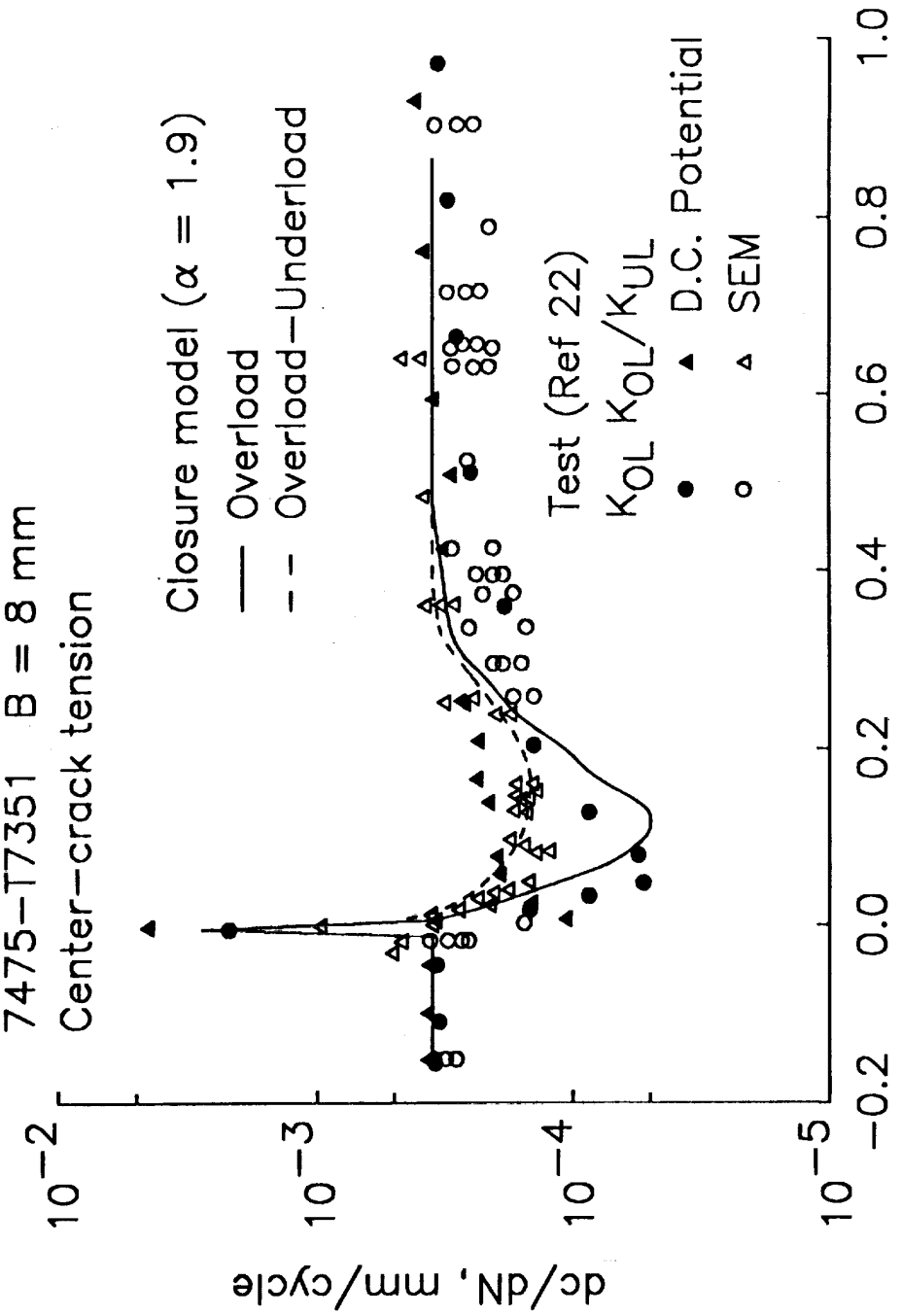

Fig. 10 Measured and predicted rates for large cracks after an overload and after an overload-underload sequence.

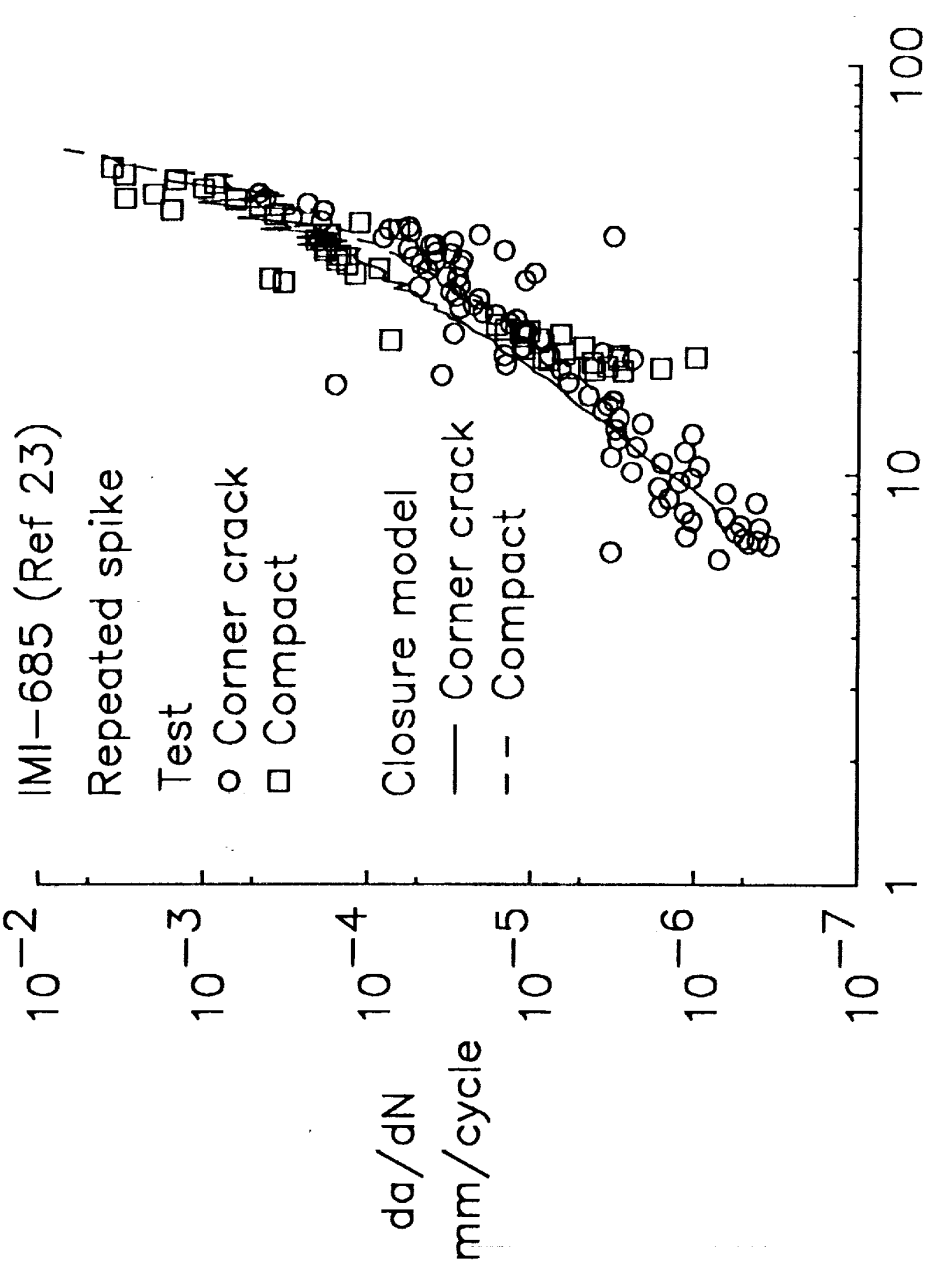

Fig. 11 Measured and predicted rates for IMI-685 titanium alloy compact and corner-crack specimens under a repeated spike overload sequence.

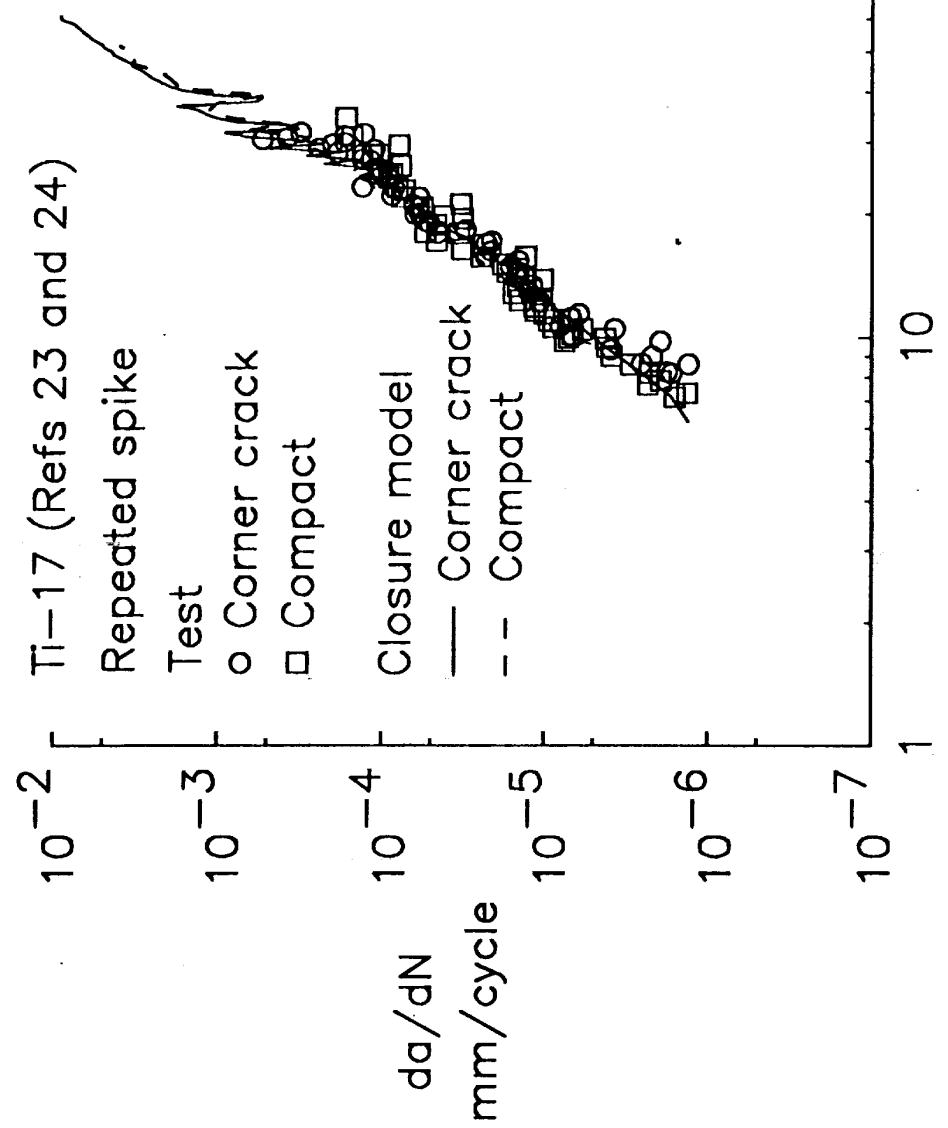

Fig. 12 Measured and predicted rates for Ti-17 titanium alloy compact and corner-crack specimens under a repeated spike overload sequence.

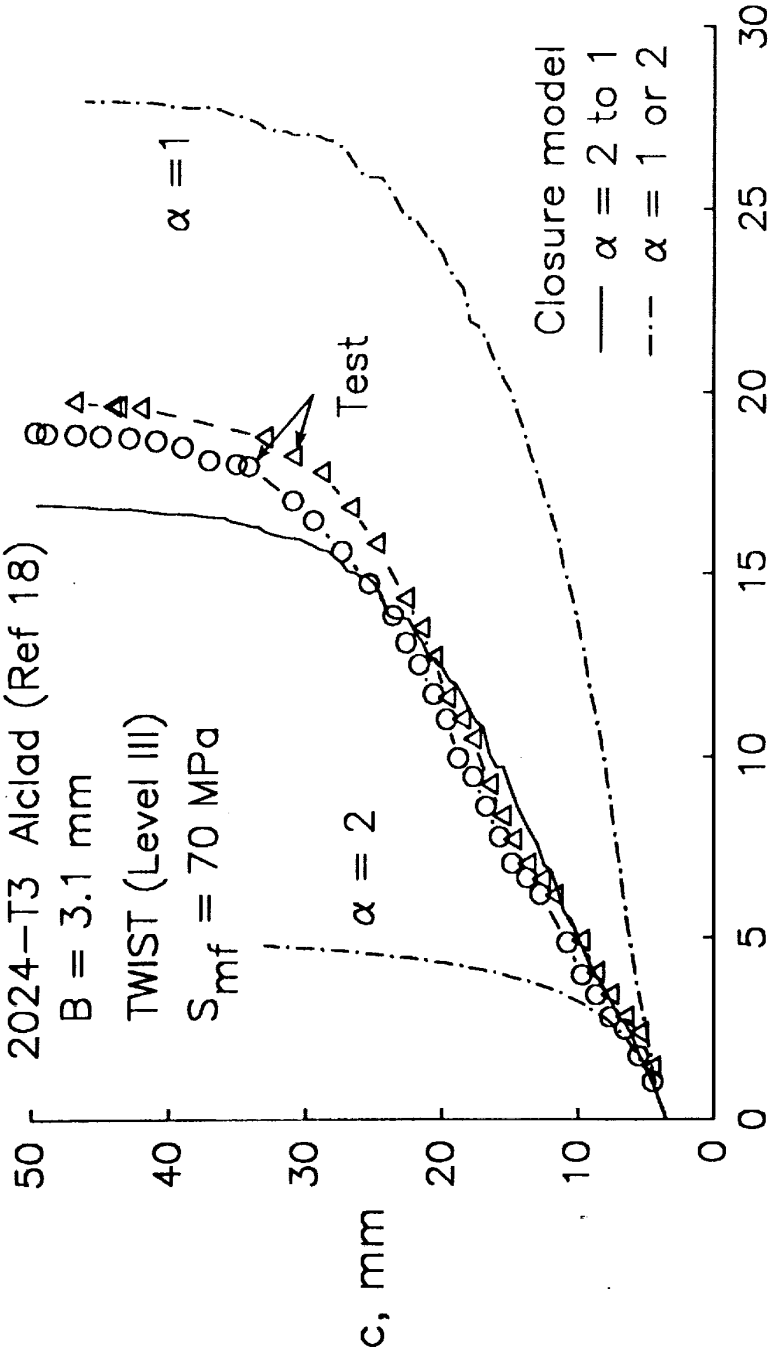

Fig. 13 Measured and calculated crack-length-against-cycles for large cracks under TWIST loading.

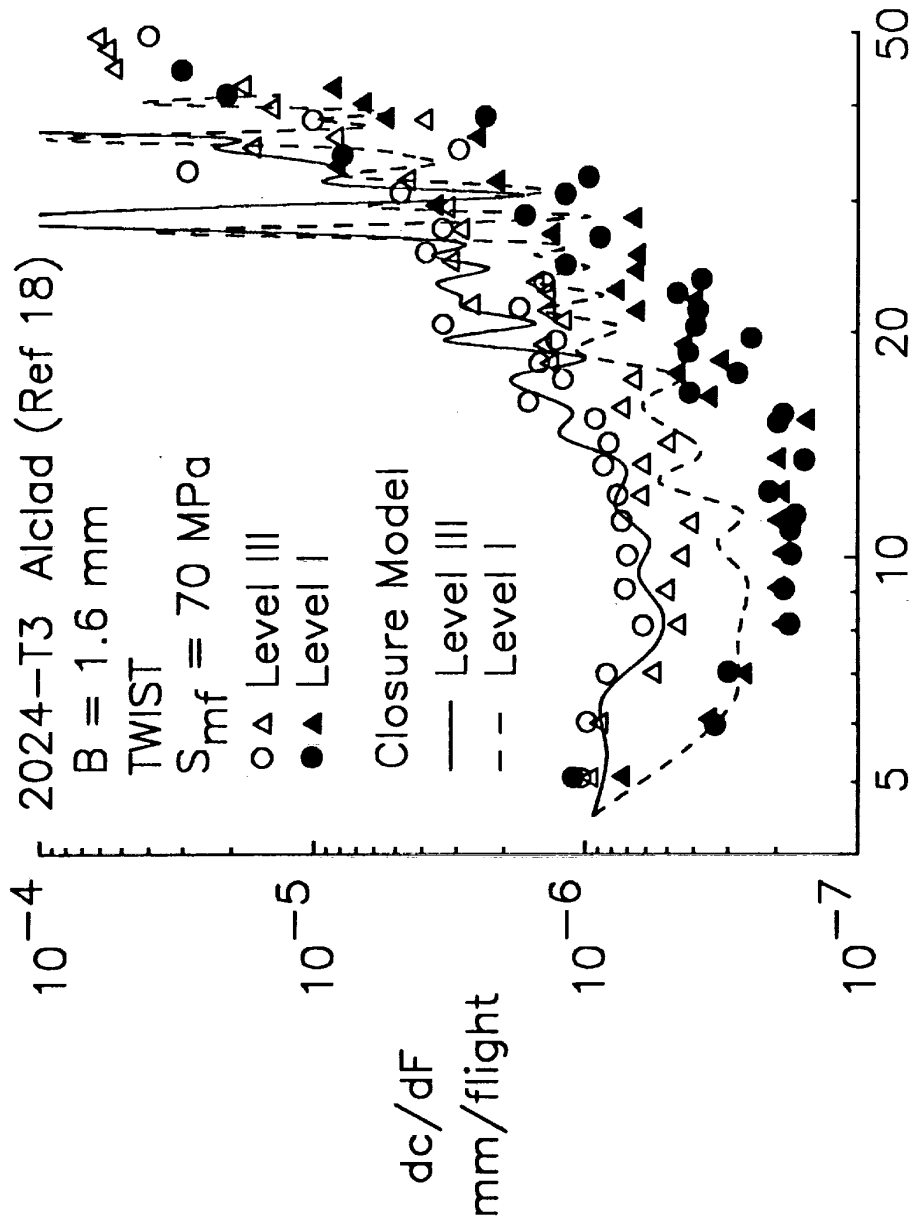

Fig. 14 Measured and calculated rates for large cracks under TWIST loading.

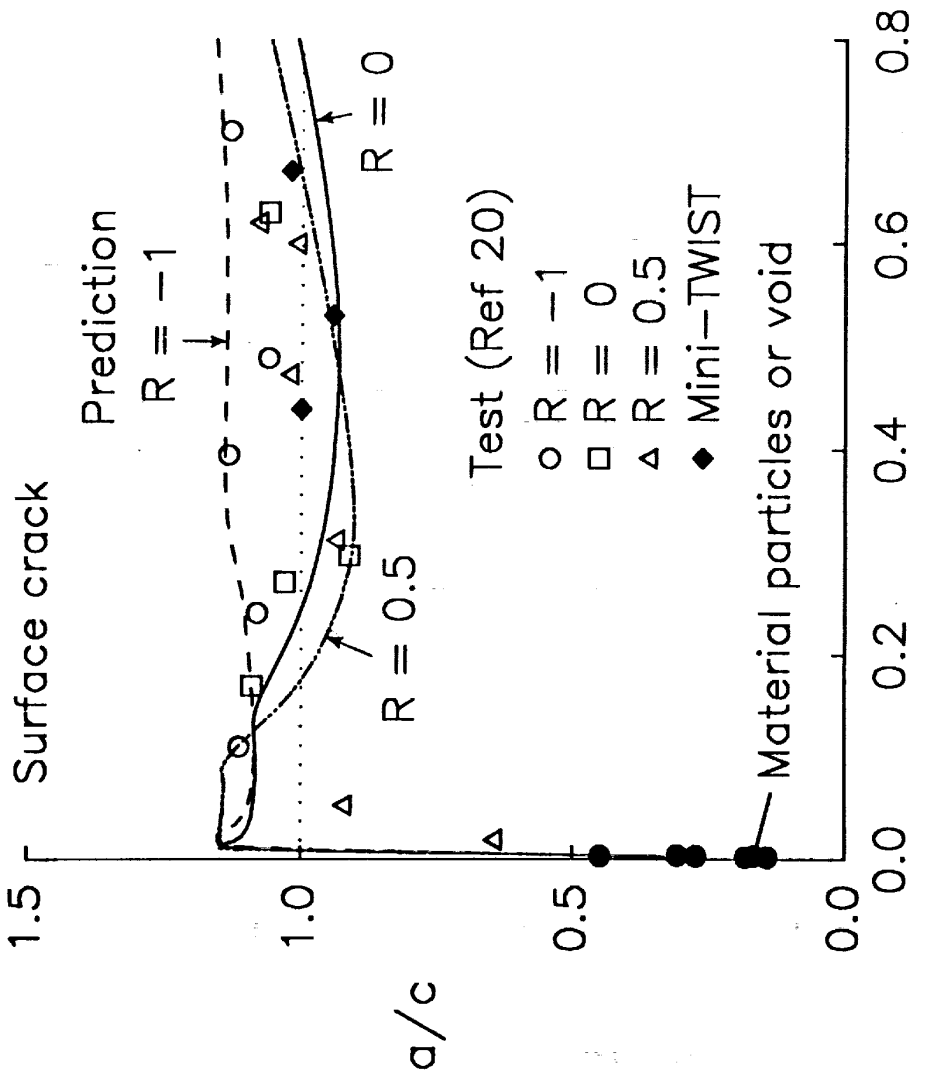

Fig. 15 Measured and predicted surface crack shape changes in 7075-T6 aluminum alloy for various stress ratios.

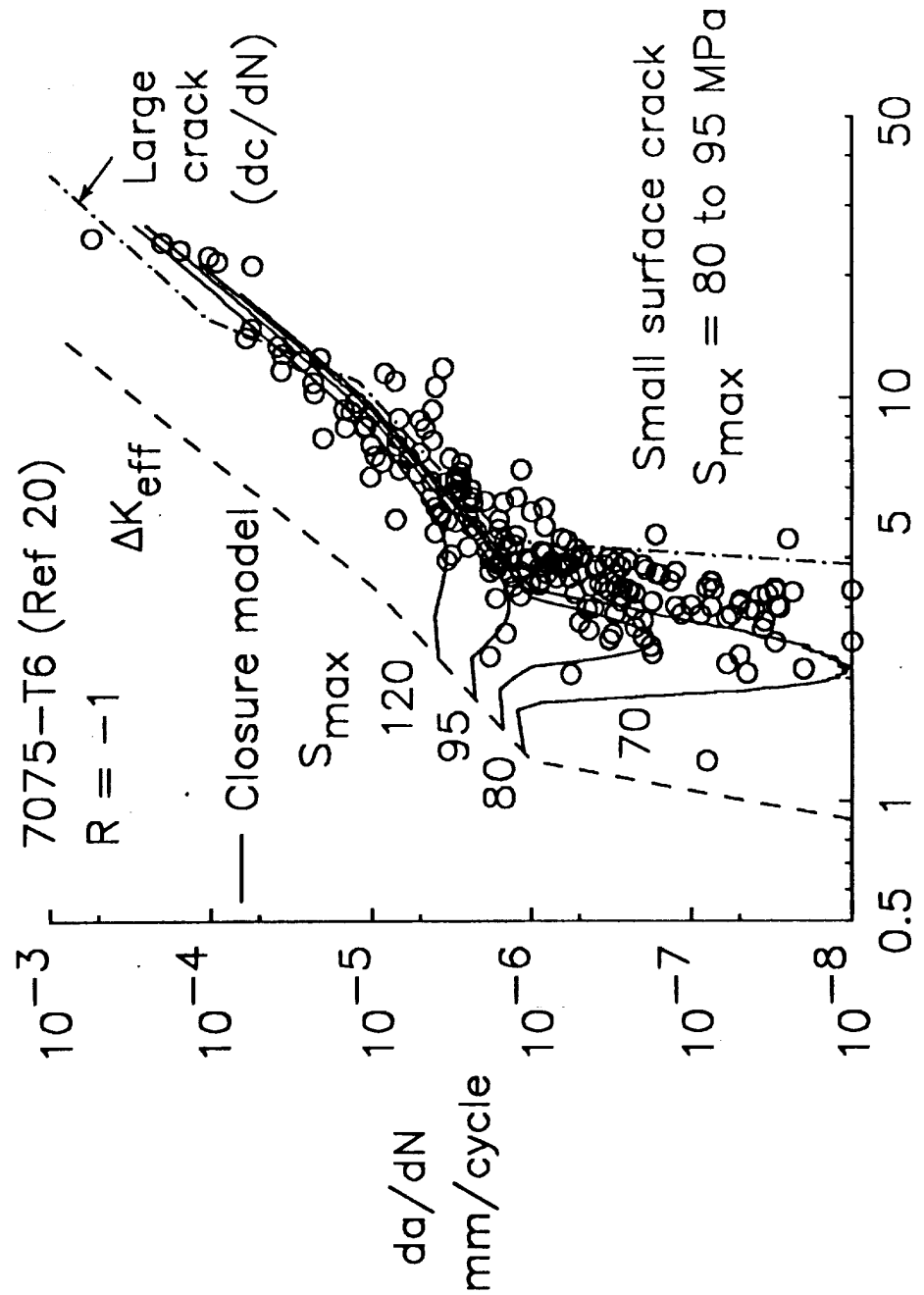

Fig. 16 Measured and predicted small surface crack growth rates against ΔK in 7075-T6 aluminum alloy under R = -1 loading.

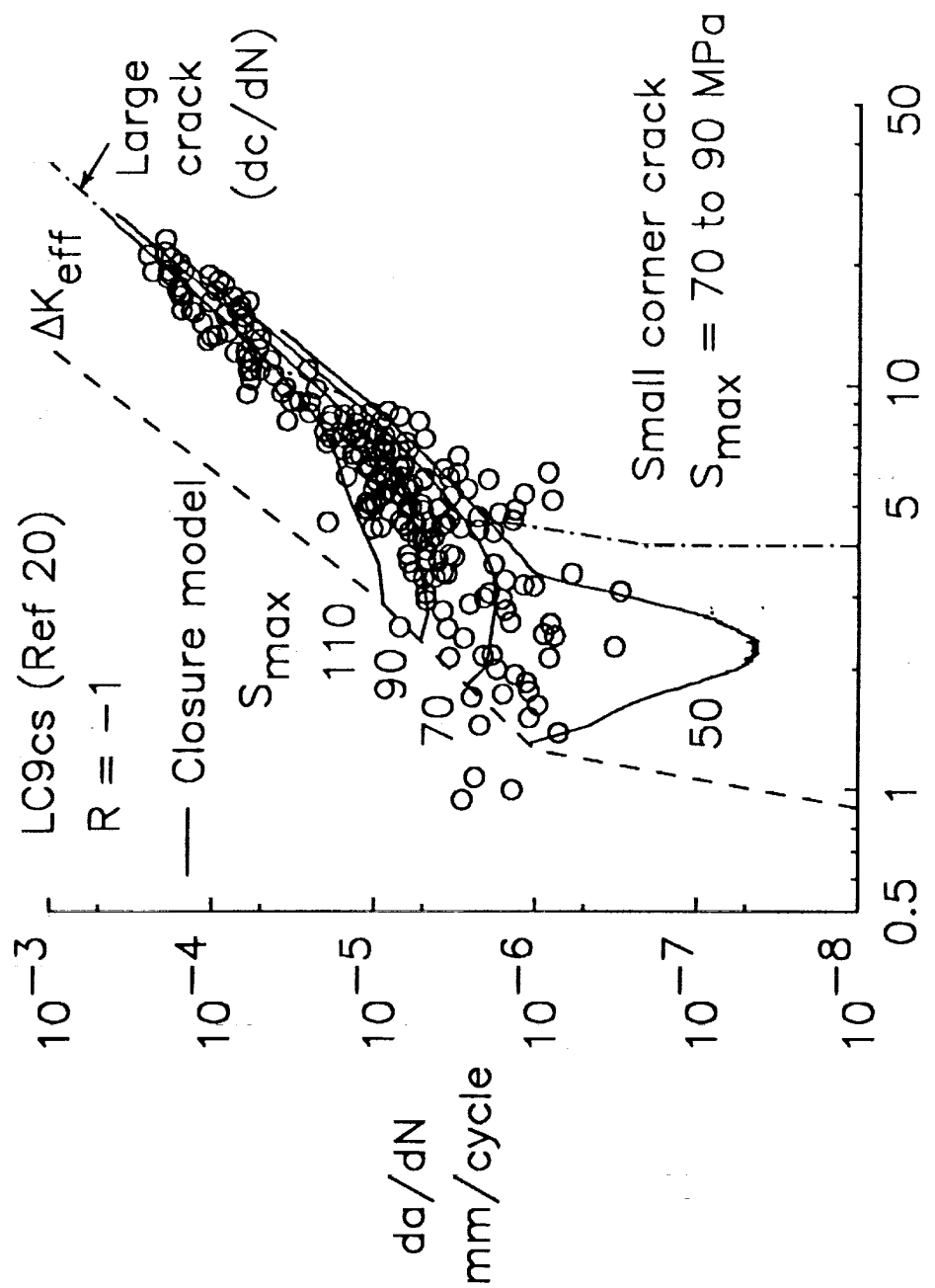

Fig. 17 Measured and predicted small surface crack growth rates against ΔK in LC9cs clad aluminum alloy under R = -1 loading.

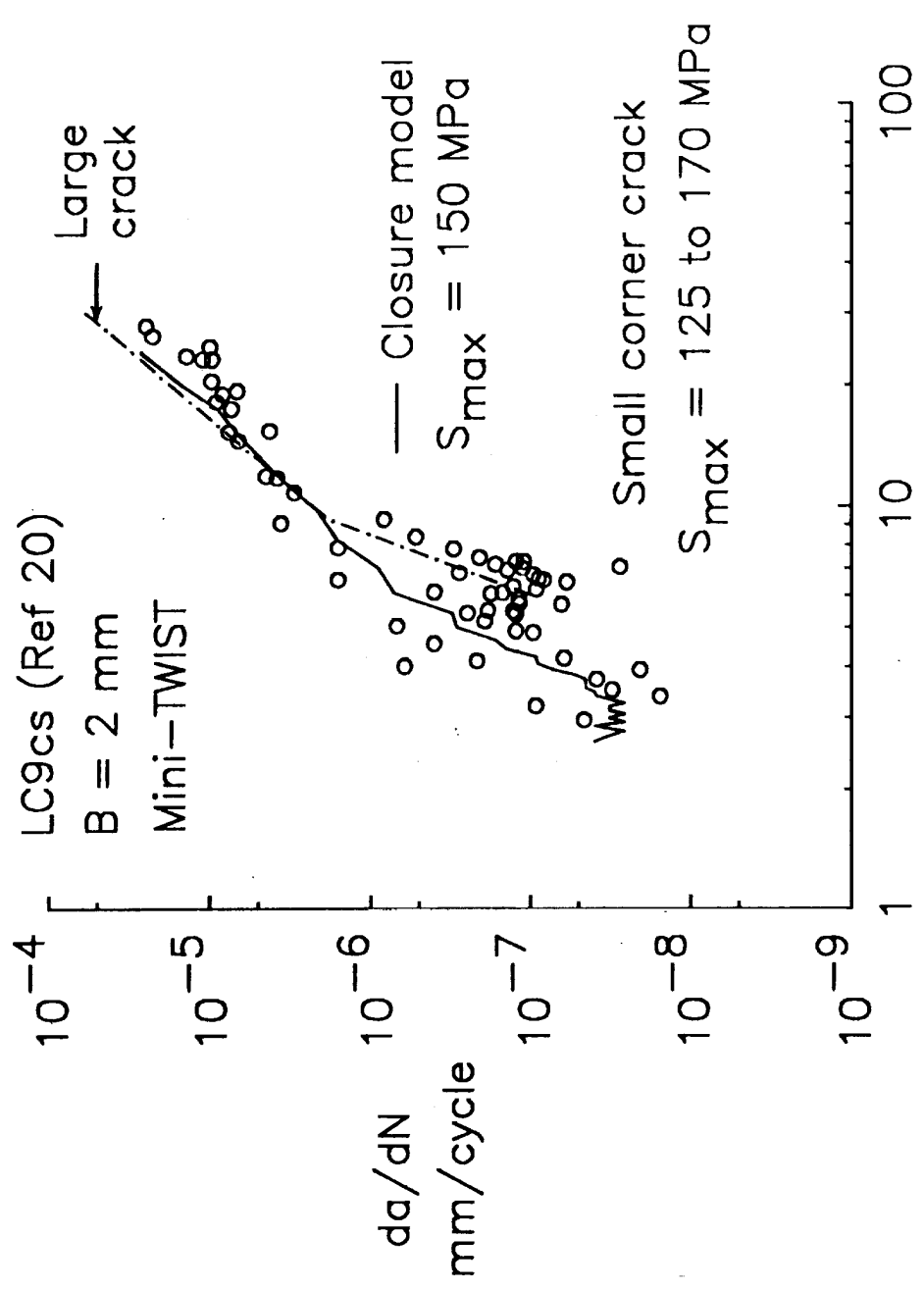

Fig. 18 Measured and predicted small surface crack growth rates against ΔK in LC9cs clad aluminum alloy under Mini-TWIST loading.

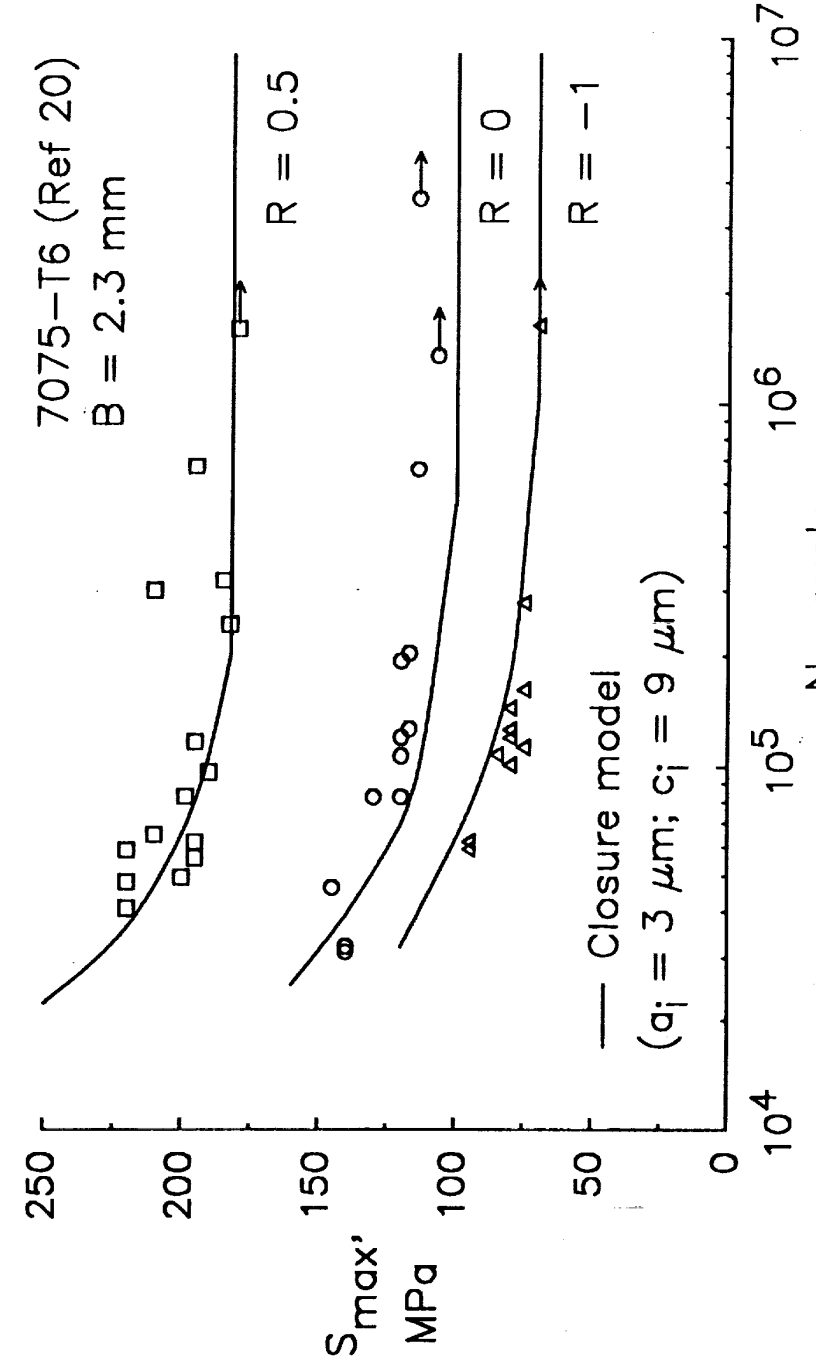

Fig. 19 Measured and predicted fatigue lives for 7075-T6 aluminum alloy SENT specimens for various stress ratios.

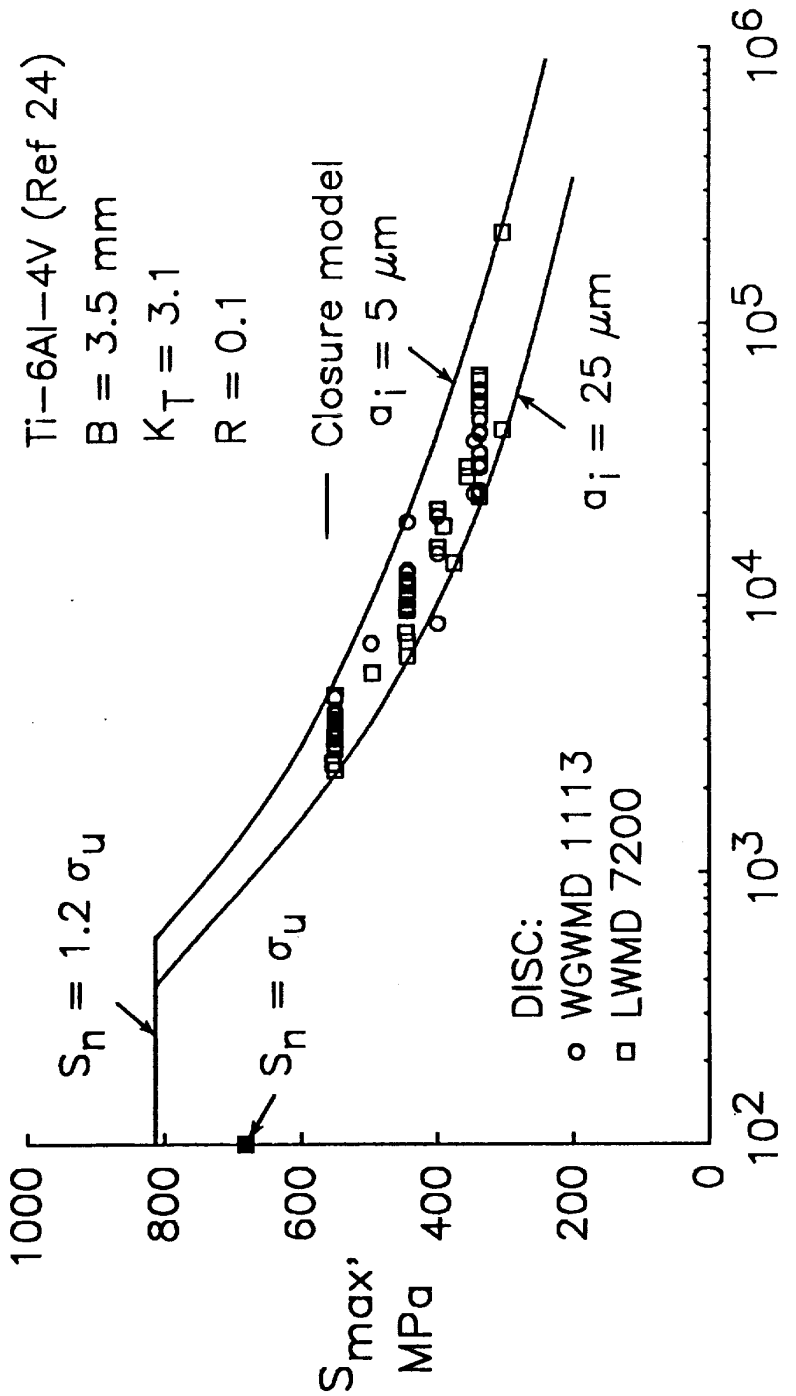

Fig. 20 Measured and predicted fatigue lives for Ti-6Al-4V titanium alloy DENT specimens.

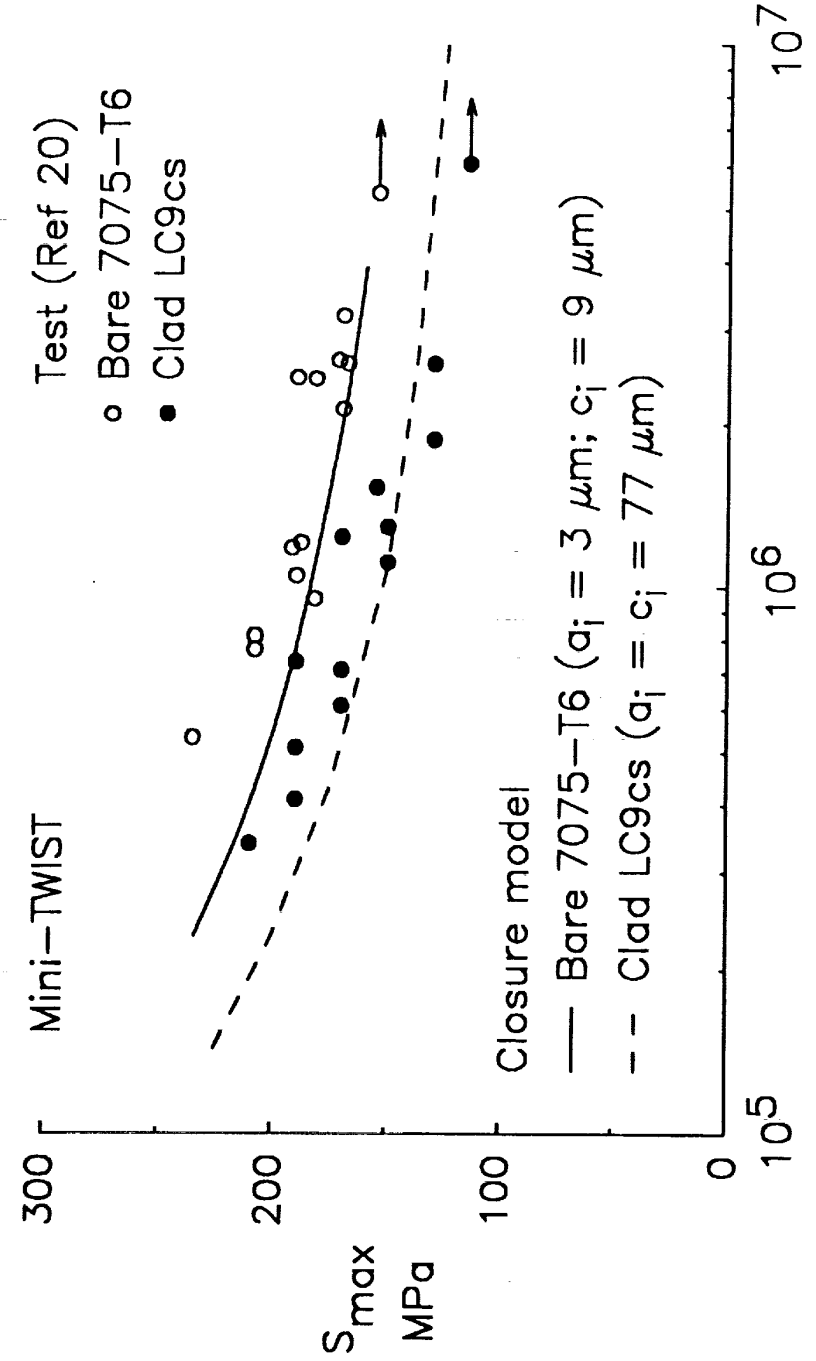

Fig. 21 Measured and predicted fatigue lives for SENT specimens made of bare and clad aluminum alloys under Mini-TWIST spectrum loading.

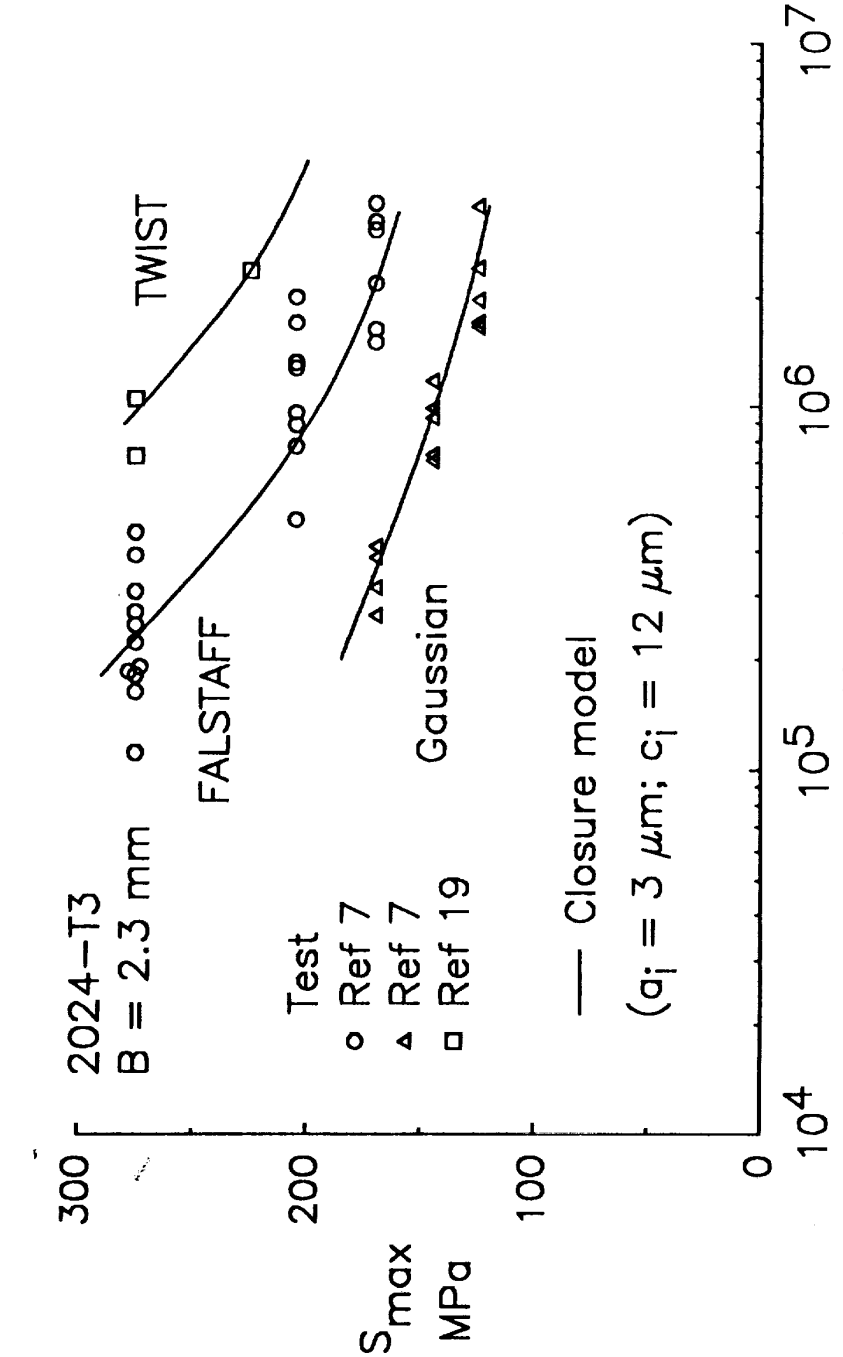

Fig. 22 Measured and predicted fatigue lives to breakthrough for SENT specimens under three spectrum loadings.

REPORT DOCUMENTATION PAGE

Form Approved
OMB No. 0704-0188

1. AGENCY USE ONLY (Leave blank)	2. REPORT DATE	3. REPORT TYPE AND DATES COVERED
	October 1993	Technical Memorandum

4. TITLE AND SUBTITLE
Fatigue Life and Crack Growth Prediction Methodology

5. FUNDING NUMBERS
WU 538-02-10-01

6. AUTHOR(S)
J. C. Newman, Jr., E. P. Phillips, and R. A. Everett, Jr.

7. PERFORMING ORGANIZATION NAME(S) AND ADDRESS(ES)
NASA Langley Research Center
Hampton, VA 23681-0001

8. PERFORMING ORGANIZATION REPORT NUMBER

9. SPONSORING / MONITORING AGENCY NAME(S) AND ADDRESS(ES)
National Aeronautics and Space Administration
Washington, DC 20546-0001

10. SPONSORING / MONITORING AGENCY REPORT NUMBER
NASA TM 109044

11. SUPPLEMENTARY NOTES
Presented at the AGARD Structures and Materials Panel Workshop on An Assessment of Fatigue Damage and Crack Growth Prediction Techniques, Bordeaux, France, September 29-30, 1993

12a. DISTRIBUTION / AVAILABILITY STATEMENT
Unclassified - Unlimited

Subject Category - 24

12b. DISTRIBUTION CODE

13. ABSTRACT *(Maximum 200 words)*

This paper reviews the capabilities of a plasticity-induced crack-closure model and life-prediction code to predict fatigue crack growth and fatigue lives of metallic materials. Crack-tip constraint factors, to account for three-dimensional effects, were selected to correlate large-crack growth rate data as a function of the effective-stress-intensity factor range (ΔK_{eff}) under constant-amplitude loading. Some modifications to the ΔK_{eff}-rate relations were needed in the near-threshold regime to fit small-crack growth rate behavior and endurance limits. the model was then used to calculate small- and large-crack growth rates, and in some cases total fatigue lives, for several aluminum and titanium alloys under constant-amplitude, variable-amplitude, and spectrum loading. Fatigue lives were calculated using the crack-growth relations and microstructural features like those that initiated cracks. Results from the tests and analyses agreed well.

14. SUBJECT TERMS
Fatigue; Crack propagation; Fracture; Small crack; Metals

15. NUMBER OF PAGES
46

16. PRICE CODE
A03

17. SECURITY CLASSIFICATION OF REPORT	18. SECURITY CLASSIFICATION OF THIS PAGE	19. SECURITY CLASSIFICATION OF ABSTRACT	20. LIMITATION OF ABSTRACT
Unclassified	Unclassified		